

# WGRIN toolbox user manual

Stéphane BALAC

Univ. Rennes, CNRS, IRMAR - UMR 6625  
F-35000 Rennes, France

Release 1.0 - September 2020

## Abstract

WGRIN is a MATLAB toolbox aimed at studying Whispering Gallery Modes (WGM) in graded index (GRIN) optical micro-resonators. Such resonators have a dielectric cavity with a spatially varying refractive index. The WGRIN toolbox deals with dielectric cavities the shape of which is a disk or a sphere and the refractive index varies with the radial position. For these two geometries, the resonance problem can be formulated in the unique form of a one-dimensional problem in the radial variable. This resonance problem is solved by the Finite Difference Method with Perfectly Matched Layer (PML). The WGRIN toolbox allows the computation of resonance wavelengths and the visualization of WGM in GRIN micro-disk and micro-sphere resonators.

---

## Contents

1	Introduction	2
1.1	A unified problem formulation for micro-disks and micro-spheres . . . . .	2
1.2	Use of a Perfectly Matched Layer . . . . .	3
1.3	Computation of the modes outside the cavity . . . . .	4
2	Discretization using a Finite Difference scheme	5
3	The WGRIN toolbox	7
3.1	Contents of the WGRIN toolbox . . . . .	7
3.2	Operating principle of the WGRIN toolbox . . . . .	8
3.3	A comprehensive test run for a micro-disk . . . . .	11
3.4	A comprehensive test run for a micro-sphere . . . . .	16
3.5	Detection of spurious resonances . . . . .	20
	References	27
	Appendix	29
A	Physical and mathematical backgrounds	29
A.1	Maxwell's equations in a GRIN micro-resonator . . . . .	29
A.2	Mathematical model for WGM in a GRIN micro-disk . . . . .	30
A.3	Mathematical model for WGM in a GRIN micro-sphere . . . . .	33

---

# 1 Introduction

## 1.1 A unified problem formulation for micro-disks and micro-spheres

Mathematical modeling of WGM in a dielectric cavity obeys a general framework given by harmonic Maxwell's equations, see Appendix A.1. In the cases of a micro-disk or micro-sphere, this general framework can be considerably simplified taking advantage of geometrical symmetries as detailed in Appendix A.2 and Appendix A.3. In the sequel, we will denote by  $R$  the radius of the micro-disk (resp. of the micro-sphere) and we will denote by  $N$  the function defining the refractive index, assumed to be dependent of the radial variable only in the cavity and to be equal to 1 outside the cavity. Although the mathematical developments are rather different in the case of a micro-disk and in the case of a micro-sphere, the final expression of the two resonance problems can be gathered into a unique formulation uniting the two cases. Namely, the resonance problems (A.13) and (A.24) (see Appendix A) obtained respectively for a micro-disk and for a micro-sphere can be combined into the following unique problem for the purpose of the numerical approximation by the Finite Difference Method: Find  $(k_q, u_q) \in \mathbb{C} \times \mathcal{D}(\mathbb{R}^+, r dr)$  such that  $\text{Im}(k_q) < 0$ ,  $u_q \neq 0$  and

$$\begin{cases} - (a(r)u_q'(r))' + b(r)u_q(r) = k_q^2 c(r)u_q(r) & \text{in } ]0, R[ \text{ and } ]R, +\infty[ & (1a) \\ u_q(0) = 0 & & (1b) \\ [u_q(R)] = 0 & & (1c) \\ [a(R)u_q'(R)] = 0 & & (1d) \end{cases}$$

where  $\mathcal{D}(\mathbb{R}^+, r dr)$  denotes the functional space

$$\mathcal{D}(\mathbb{R}^+, r dr) = \{v \in L_{\text{loc}}^2(\mathbb{R}^+, r dr) \mid v|_{]0, R[} \in \mathbf{H}^2(]0, R[, r dr), v|_{]R, +\infty[} \in \mathbf{H}_{\text{loc}}^2(]R, +\infty[, r dr)\}$$

with  $L_{\text{loc}}^2(\mathbb{R}^+, r dr)$  denoting the Lebesgue set of locally square integrable functions in  $\mathbb{R}^+$  with respect to the measure  $r dr$  and  $\mathbf{H}^2(]0, R[, r dr)$  (resp.  $\mathbf{H}_{\text{loc}}^2(]R, +\infty[, r dr)$ ) denoting the Sobolev space of square integrable functions in  $]0, R[$  (resp. in  $]R, +\infty[$ ) with all derivatives up to order 2 in  $L^2(]0, R[, r dr)$  (resp. in  $L_{\text{loc}}^2(]R, +\infty[, r dr)$ ), and where

- for a micro-disk:  $q = m$  is the polar mode index and we have  
 $a : r \in ]0, +\infty[ \mapsto rN^{p-1}(r)$ ,  $b : r \in ]0, +\infty[ \mapsto \frac{m}{r}N^{p-1}(r)$ ,  $c : r \in ]0, +\infty[ \mapsto rN^{p+1}(r)$ ;
- for a micro-sphere:  $q = \ell$  is the polar mode index and we have  
 $a : r \in ]0, +\infty[ \mapsto N^{p-1}(r)$ ,  $b : r \in ]0, +\infty[ \mapsto \frac{\ell(\ell+1)}{r^2}N^{p-1}(r)$ ,  $c : r \in ]0, +\infty[ \mapsto N^{p+1}(r)$ .

Note that with the usual convention for naming TE and TM modes in a micro-disk and in a micro-sphere [3], the value of the parameter  $p$  in the definition of the coefficient functions  $a$ ,  $b$  and  $c$  is as follows:

- for a micro-disk,  $p = -1$  for TE modes and  $p = 1$  for TM modes;
- for a micro-sphere,  $p = -1$  for TM modes and  $p = 1$  for TE modes.

For a micro-disk,  $u_q$  coincides with the solution  $u_m$  to problem (A.13) whereas for a micro-sphere,  $u_q$  coincides with the solution  $S_\ell$  to problem (A.24). The condition at infinity reads

- for a micro-disk:  $u_q(r) = u_m(r) \propto \mathbf{H}_m^{(1)}(kr)$  as  $r \rightarrow +\infty$ , where  $\mathbf{H}_m^{(1)}$  denotes Hankel function of the first kind [1, 2];
- for a micro-sphere:  $u_q(r) = S_\ell(r) \propto \xi_\ell(kr)$  as  $r \rightarrow +\infty$ , where  $\xi_\ell$  denotes Riccati-Bessel function [1, 2] defined by  $\xi_\ell(z) = \sqrt{\frac{\pi z}{2}} \mathbf{H}_{\ell+\frac{1}{2}}^{(1)}(z)$ .

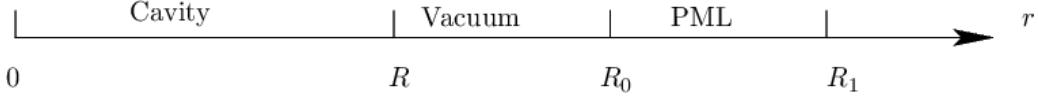


Figure 1: Notation used for defining the PML. In the WGRIN toolbox, the choice  $R_0 = R$  is made.

Details on the way mode indexes for a micro-disk and a micros-sphere are defined can be found in the appendix, respectively on p. 33 and on p. 36.

For a general radial varying refractive index function  $N$ , it is not possible to find closed-form solutions to problem (1) and a numerical approximation method is mandatory to compute approximate solutions to problem (1). Among the classical numerical methods for such a boundary value problem are the Finite Element Method (FEM) and the Finite Difference Method (FDM). In the WGRIN toolbox, we have chosen to implement the Finite Difference Method because of its simplicity.

## 1.2 Use of a Perfectly Matched Layer

Since the resonance problem (1) is set in an unbounded domain, it is mandatory to bound the computational domain in order to use the FDM. This can be done by introducing a fictitious boundary at a given distance from the dielectric cavity boundary and by imposing a homogeneous Dirichlet boundary condition as in [4]. This approach has one major drawback: the resonances for the new problem set in the bounded domain are real numbers. This means that there is no way to approximate the imaginary part of the resonances in proceeding in this way. An alternative approach consists in using Perfectly Matched Layer (PML) that are now widely used to approximate solutions of wave-propagation problems in unbounded domains [5]. The WGRIN toolbox uses the PML method investigated in [6] for resonance problems, see also [7]. Let us sketch the method. Let  $R_0$  be a positive number defining the PML inner side such that  $R_0 \geq R$  and let  $R_1$  be another positive number defining the PML outer side such that  $R_1 > R_0$ , see Fig. 1. The PML approximation can be thought of as a formal complex shift in coordinate system [5]. We define a complex shift variable  $\tilde{r} \stackrel{\text{def}}{=} r(1 + i\tilde{\sigma}(r))$  where the function  $\tilde{\sigma}$  satisfies

$$\tilde{\sigma}(r) = \begin{cases} 0 & \text{for } 0 \leq r \leq R_0 \\ \frac{\sigma_0}{\sigma_1} \int_{R_0}^r f_{\aleph}(t) dt & \text{for } R_0 < r \leq R_1 \end{cases} \quad (2)$$

where  $\sigma_0 > 0$  is a parameter of the PML,  $\sigma_1 = \int_{R_0}^{R_1} f_{\aleph}(t) dt$  and  $f_{\aleph}$  is the polynomial function  $t \in \mathbb{R} \mapsto (t - R_0)^{\aleph}(R_1 - t)^{\aleph}$  where the integer  $\aleph \geq 2$  is an other adjustable parameter of the PML. One can show that the regularity of  $\tilde{\sigma}$  is directly related to the value of  $\aleph$  since  $\tilde{\sigma} \in \mathcal{C}^{\aleph}([0, R_1])$ . The condition  $\aleph \geq 2$  is imposed for the complex shift in coordinates detailed below to hold.

We shall use the following notations for  $r \geq 0$

$$\begin{aligned} \tilde{d}(r) &\stackrel{\text{def}}{=} 1 + i\tilde{\sigma}(r) \\ \sigma(r) &\stackrel{\text{def}}{=} \frac{\partial(r\tilde{\sigma}(r))}{\partial r} = \tilde{\sigma}(r) + r \frac{\partial\tilde{\sigma}(r)}{\partial r} = \begin{cases} 0 & r \leq R_0 \\ \tilde{\sigma}(r) + r \frac{\sigma_0}{\sigma_1} f_{\aleph}(r) & R_0 < r < R_1 \end{cases} \end{aligned}$$

With these notations, we have  $\tilde{r}(r) = r\tilde{d}(r)$  and

$$d(r) \stackrel{\text{def}}{=} \frac{\partial\tilde{r}(r)}{\partial r} = 1 + i\sigma(r).$$

Note that the complex shift operates for  $r > R_0$  and leaves unchanged the variable in  $[0, R_0]$  (i.e.  $\tilde{r} = r$ ). Equation (1a) in the shift variable  $\tilde{r}$  reads

$$-\partial_{\tilde{r}}(a(\tilde{r})\partial_{\tilde{r}}u_q(\tilde{r})) + b(\tilde{r})u_q(\tilde{r}) = k_q^2 c(\tilde{r})u_q(\tilde{r}) \quad (3)$$

We introduce as new unknown the function  $\tilde{u}_q$  defined by  $\tilde{u}_q(r) = u_q(\tilde{r}), \forall r \geq 0$ , and we denote by  $\tilde{N}$  the function such that  $\tilde{N}(r) = N(\tilde{r}), \forall r \geq 0$ . Equation (3) for  $\tilde{u}_q$  reads

$$-(\tilde{a}(r)\tilde{u}'_q(r))' + \tilde{b}(r)u_q(r) = k_q^2 \tilde{c}(r)u_q(r)$$

where

- for a micro-disk:  $\tilde{a} : r \in ]0, +\infty[ \mapsto r \frac{d(r)}{d(\tilde{r})} N^{p-1}(r\tilde{d}(r)), \tilde{b} : r \in ]0, +\infty[ \mapsto \frac{m^2 d(r)}{r} \frac{d(r)}{d(\tilde{r})} N^{p-1}(r\tilde{d}(r)),$   
 $\tilde{c} : r \in ]0, +\infty[ \mapsto r\tilde{d}(r)d(r)N^{p+1}(r\tilde{d}(r));$
- for a micro-sphere:  $\tilde{a} : r \in ]0, +\infty[ \mapsto \frac{1}{d(\tilde{r})} N^{p-1}(r\tilde{d}(r)), \tilde{b} : r \in ]0, +\infty[ \mapsto \frac{\ell(\ell+1)}{r^2} \frac{d(r)}{d^2(\tilde{r})} N^{p-1}(r\tilde{d}(r)),$   
 $\tilde{c} : r \in ]0, +\infty[ \mapsto d(r)N^{p+1}(r\tilde{d}(r)).$

An important question to be addressed is where the PML has to be placed. Although it can be theoretically placed at any position outside the cavity, numerical investigations have shown us that less spurious resonances are obtained in the extreme case when  $R_0 = R$ , that is to say when the PML adjoins the dielectric cavity. This is therefore the situation envisaged in the WGRIN toolbox.

The interface conditions (1c) and (1d) at the dielectric cavity boundary become

$$\tilde{u}_q(R^-) = \tilde{u}_q(R^+) \quad (4a)$$

$$\tilde{a}(R^-)\tilde{u}'_q(R^-) = \tilde{a}(R^+)\tilde{u}'_q(R^+) \quad (4b)$$

where we have used the notation  $u_q(R^-) = \lim_{r \nearrow R} u_q(r)$  and  $u_q(R^+) = \lim_{r \searrow R} u_q(r)$ . (Note that the same notations will be used throughout the paper.) At the PML end, we impose the Dirichlet boundary condition  $\tilde{u}_q(R_1) = 0$ .

Finally, we have to deal with the following approximate problem deduced from (1) where the computational domain is bounded at  $r = R_1$  and a PML is used in the interval  $[R, R_1]$ : Find  $(\tilde{k}_q, \tilde{u}_q) \in \mathbb{C} \times D([0, R_1], r dr)$  such that  $\text{Im}(\tilde{k}_q) < 0, \tilde{u}_q \neq 0$  and

$$\left\{ \begin{array}{l} -(\tilde{a}(r)\tilde{u}'_q(r))' + \tilde{b}(r)u_q(r) = \tilde{k}_q^2 \tilde{c}(r)u_q(r) \quad \text{in } ]0, R[ \text{ and } ]R, R_1[ \quad (5a) \\ \tilde{u}_q(R^-) = \tilde{u}_q(R^+) \quad (5b) \\ \tilde{a}(R^-)\tilde{u}'_q(R^-) = \tilde{a}(R^+)\tilde{u}'_q(R^+) \quad (5c) \\ \tilde{u}_q(0) = 0 \quad (5d) \\ \tilde{u}_q(R_1) = 0 \quad (5e) \end{array} \right.$$

From now on, the solutions to problem (5) will be denoted by  $(k_q, u_q)$  for the sake of simplicity.

### 1.3 Computation of the modes outside the cavity

We found that an effective way of reducing the number of spurious resonances among the computed resonances was to position the PML entry at the dielectric cavity boundary. This choice implies that the modes are not computed by the FDM outside the dielectric cavity. Yet, it is sometimes helpful to have a graphical representation of the modes outside the cavity. This can be done at a low computational cost from the values of the modes computed at the dielectric cavity boundary as detailed below.

### 1.3.1 Case of a micro-disk

The mathematical modeling for resonances in a disk shaped dielectric cavity is detailed in Appendix A.2, see problem (A.13). In the exterior domain  $]R, +\infty[$ , the unknown  $u_q \equiv u_m$  in problem (1) satisfies

$$u_m''(r) - \frac{1}{r}u_m'(r) + \left(\frac{m^2}{r^2} - k_m^2\right)u_m(r) = 0. \quad (6)$$

This second order ordinary differential equation is referred to as a Bessel's equation of order  $m$  (after the change of variables  $x = k_m r$ ). The space of solutions admits a basis formed e.g. by the two linearly independent Hankel functions of first and second kinds,  $H_m^{(1)}$  and  $H_m^{(2)}$ . As well known, under the  $e^{-i\omega t}$  convention for harmonic time dependence of the electromagnetic field adopted here, Hankel function  $H_m^{(1)}$  represents outgoing waves whereas  $H_m^{(2)}$  represents ingoing waves. Thus, outside the disk, the mode  $u_m$  for a given resonance  $k_m$  can be expressed as

$$u_m(r) = u_m(R) \frac{H_m^{(1)}(k_m r)}{H_m^{(1)}(k_m R)} \quad \forall r > R. \quad (7)$$

### 1.3.2 Case of a micro-sphere

The mathematical modeling for resonances in a spherical dielectric cavity is detailed in Appendix A.3, see problem (A.24). In the exterior domain  $]R, +\infty[$ , the unknown  $u_q \equiv S_\ell$  in problem (1) satisfies

$$-S_\ell''(r) + \left(\frac{\ell(\ell+1)}{r^2} - k_\ell^2\right)S_\ell(r) = 0. \quad (8)$$

This second order ordinary differential equation is referred to a Ricatti-Bessel's equation of order  $\ell$  (consider the change of variables  $x = k_\ell r$ ). Taking into account the outgoing wave condition at infinity, the solution to equation (8) can be expressed in terms of Ricatti-Bessel function  $\xi_\ell$  defined as  $\xi_\ell(x) = \sqrt{\frac{\pi x}{2}}H_{\ell+\frac{1}{2}}^{(1)}(x)$ . Thus, outside the sphere, the mode  $S_\ell$  for a given resonance  $k_\ell$  can be expressed as

$$S_\ell(r) = S_\ell(R) \frac{\xi_\ell(kr)}{\xi_\ell(kR)} \quad \forall r > R. \quad (9)$$

## 2 Discretization using a Finite Difference scheme

The WGRIN toolbox solves problem (5) using the Finite Difference Method (FDM) where the derivative of a given function  $v$  with regularity  $C^1$  is approached by the following second-order of accuracy central difference formula (for a small step-size  $\delta_r > 0$ )

$$v'(r) \approx \frac{v(r + \frac{1}{2}\delta_r) - v(r - \frac{1}{2}\delta_r)}{\delta_r}. \quad (10)$$

We introduce a subdivision  $(r_j)_{j=0,\dots,J}$  with constant step-size  $\delta_r = R_1/J$  of the computational domain  $[0, R_1]$  satisfying the following constraint: There exists an integer  $J_R$  such that  $R = J_R\delta_r$ , see Fig. 2. This assumption ensures that the cavity boundary located at  $r = R$  coincides with a subdivision node. For  $j = 1, \dots, J-1$ ,  $j \neq J_R$ , using (10) successively with  $v = u_q$  and  $v = au'_q$ , equation (5a) gives rise to the following discrete equation

$$\frac{1}{\delta_r^2} \left( (\tilde{a}(r_j + \frac{\delta_r}{2}) + \tilde{a}(r_j - \frac{\delta_r}{2}))u_j - \tilde{a}(r_j - \frac{\delta_r}{2})u_{j-1} - \tilde{a}(r_j + \frac{\delta_r}{2})u_{j+1} \right) + \tilde{b}(r_j)u_j = k_q^2 \tilde{c}(r_j)u_j$$

where  $u_j$  denotes the approximation of  $u_q(r_j)$  and where from the boundary condition (5d), we have set  $u_0 = 0$ .

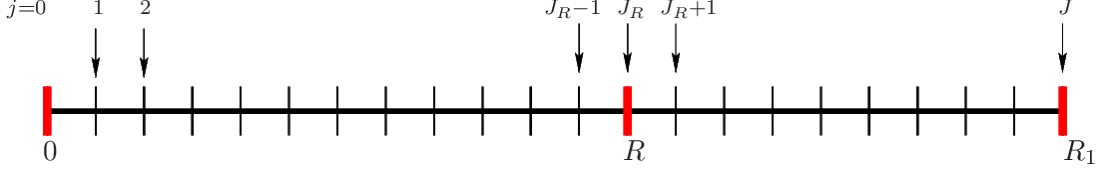


Figure 2: Notation used for the discretization. The index  $j$  labels the discretization nodes.

The boundary condition (5b) reflects the continuity of the solution  $\tilde{u}_q$  across the interface located at  $r = R$ . Therefore, only one unknown is required to describe the solution at the interface. In order to build a second order approximation of the boundary condition (5c), we proceed as follows. On the one hand, from Taylor expansion formula, we have with an error in  $\mathcal{O}(\delta_r^2)$ ,

$$(\tilde{a} u'_q)(R - \frac{\delta_r}{2}) = (\tilde{a} u'_q)(R^-) - \frac{\delta_r}{2} (\tilde{a} u'_q)'(R^-) \quad (11a)$$

$$(\tilde{a} u'_q)(R + \frac{\delta_r}{2}) = (\tilde{a} u'_q)(R^+) + \frac{\delta_r}{2} (\tilde{a} u'_q)'(R^+) \quad (11b)$$

and from the finite difference formula (10), we have with an error in  $\mathcal{O}(\delta_r^2)$ ,

$$(\tilde{a} u'_q)(R - \frac{\delta_r}{2}) = \tilde{a}(R - \frac{\delta_r}{2}) \frac{u_q(R) - u_q(R - \delta)}{\delta_r} \quad (12a)$$

$$(\tilde{a} u'_q)(R + \frac{\delta_r}{2}) = \tilde{a}(R + \frac{\delta_r}{2}) \frac{u_q(R + \delta) - u_q(R)}{\delta_r}. \quad (12b)$$

Combining (11) with (12), the boundary condition (5c) gives rise to the relation

$$\tilde{a}(R - \frac{\delta_r}{2}) \frac{u_q(R) - u_q(R - \delta)}{\delta_r} + \frac{\delta_r}{2} (\tilde{a} u'_q)'(R^-) = \tilde{a}(R + \frac{\delta_r}{2}) \frac{u_q(R + \delta) - u_q(R)}{\delta_r} - \frac{\delta_r}{2} (\tilde{a} u'_q)'(R^+). \quad (13)$$

On the other hand, taking into account the differential equation (5a) in the inner limit when  $r$  tends to  $R$  (resp. the outer limit when  $r$  tends to  $R$ ), we obtain

$$(\tilde{a} u'_q)'(R^-) = \tilde{b}(R^-) u_q(R) - k_q^2 \tilde{c}(R^-) u_q(R) \quad (14a)$$

$$(\tilde{a} u'_q)'(R^+) = \tilde{b}(R^+) u_q(R) - k_q^2 \tilde{c}(R^+) u_q(R). \quad (14b)$$

Finally, combining (13) with (14), we obtain the following relation with an error in  $\mathcal{O}(\delta_r^2)$

$$\frac{1}{\delta_r^2} \left( (\tilde{a}(R - \frac{\delta_r}{2}) + \tilde{a}(R + \frac{\delta_r}{2})) u_q(R) - \tilde{a}(R - \frac{\delta_r}{2}) u_q(R - \delta) - \tilde{a}(R + \frac{\delta_r}{2}) u_q(R + \delta) \right) + \frac{1}{2} (\tilde{b}(R^-) + \tilde{b}(R^+)) u_q(R) = \frac{1}{2} k_q^2 (\tilde{c}(R^-) + \tilde{c}(R^+)) u_q(R). \quad (15)$$

It follows that the boundary condition (5c) is discretized into

$$\frac{1}{\delta_r^2} \left( (\tilde{a}(R + \frac{\delta_r}{2}) + \tilde{a}(R - \frac{\delta_r}{2})) u_{J_R} - \tilde{a}(R - \frac{\delta_r}{2}) u_{J_{R-1}} - \tilde{a}(R + \frac{\delta_r}{2}) u_{J_{R+1}} \right) + \frac{1}{2} (\tilde{b}(R^-) + \tilde{b}(R^+)) u_{J_R} = \frac{1}{2} k_q^2 (\tilde{c}(R^-) + \tilde{c}(R^+)) u_{J_R}. \quad (16)$$

The discrete resonance problem obtained above can be written in matrix form as the following eigenvalue problem: Find  $V \in \mathbb{C}^{J-1}$ ,  $V \neq 0$ , and  $k_q \in \mathbb{C}$  such that

$$A V = k_q^2 C V \quad (17)$$



- `rspurious.m` : Graphic representation of the eigenvectors in the cavity and in the outer PML domain (useful to identify spurious resonances);
- `rspectrum.m` : Graphic representation of the spectrum of the Finite Difference matrix (useful to identify spurious resonances);
- MATLAB functions for the computation of WGM in a micro-sphere;
  - `slegend.m` : Associated Legendre function with Schmidt semi-normalization  $S_\ell^m$ ;
  - `dslegend.m` : Derivative of the associated Legendre function with Schmidt semi-normalization  $(S_\ell^m)'$ ;
  - `hansenm.m` : Hansen solution  $\mathbf{M}_\ell^m$  of the spherical vectorial wave equation;
  - `hansenn.m` : Hansen solution  $\mathbf{N}_\ell^m$  of the spherical vectorial wave equation;
  - `modefield.m` : Computes the amplitude of the electromagnetic field for a mode in a micro-sphere;
- Low level internal functions:
  - `matrice.m` : Computes the Finite Difference matrix;
  - `insigmat.m` : Computes the PML function  $\tilde{\sigma}$  by quadrature;
  - `info.log.m` : Gives information on the software used (MATLAB or OCTAVE) and on the standard toolboxes available.

### 3.2 Operating principle of the WGRIN toolbox

First of all, in order to use the WGRIN toolbox, the user must define the refractive index profile  $N$  in the file `optindex.m` in the form of a MATLAB handle function. For instance, for a micro-disk or micro-sphere with refractive index

$$N(r) = \frac{2n_0}{1 + (r/R)^2}$$

with vacuum outside ( $N = 1$ ), the user must provide in the file `optindex.m` the following MATLAB handle function:

```
N=@(r) 2*n0./(1+(r./R).^2).*(r<=R)+(r>R);
```

The value  $n_0$  is provided by the user at the WGRIN prompt in the MATLAB console.

For a micro-disk or micro-sphere with constant refractive index  $N = n_0$  in vacuum ( $N = 1$  outside the cavity), the user must provide in the file `optindex.m` the following MATLAB handle function:

```
N=@(r) n0*(r<=R)+(r>R);
```

It is important to declare the function  $N$  such that a vector call is possible, see the Vectorization section in the MATLAB documentation.<sup>1</sup> An important assumption on the refractive index  $N$  is that it must correspond to a smooth function of the radial position. In that respect, the WGRIN program can not deal with the case of a micro-ring considered as a disk with a piece-wise constant refractive index.<sup>2</sup>

At the WGRIN prompt, the user must indicate the geometry of the cavity (disk or sphere), its radius and the value  $n_0$  of the refractive index at the cavity boundary. He also supplies the features of the modes : TE or TM, and its polar mode index ( $m$  for a disk or  $\ell$  for a sphere).

<sup>1</sup>Available online at [https://fr.mathworks.com/help/matlab/matlab\\_prog/vectorization.html](https://fr.mathworks.com/help/matlab/matlab_prog/vectorization.html)

<sup>2</sup>This could be a subject of future developments of the code.

The WGRIN program builds the matrices  $A$  and  $C$  resulting from the Finite Difference discretization of problem (5) and solves the eigenvalue problem (17). Note that the need to bound the computational domain and the Finite Difference discretization itself are liable for the presence of spurious resonances among the eigenvalues obtained by solving (17). These spurious resonances do not have any physical meaning. Moreover, because the step-size  $\delta_r$  must be sufficiently small in order to compute accurate approximation of the resonances, the size of the matrix  $C^{-1}A$  is large and as a consequence the number of its eigenvalues too. Therefore, it is expensive and not recommended to compute all the eigenvalues of  $C^{-1}A$ . On the contrary, we must restrict ourselves to the computation of a few of them, corresponding to the look after resonances. For this purpose, in the WGRIN toolbox the number  $N_{\text{res}}$  of eigenvalues to be computed must be provided by the user as well as a guess  $\lambda_t$  for the resonance wavelengths of interest (also referred to as the target value) to indicate the position in the spectrum of the matrix  $C^{-1}A$  around which the  $N_{\text{res}}$  eigenvalues must be computed. Namely, the WGRIN toolbox uses MATLAB function `eigs` with a call in the form `eigs(A,Nres,sigma)` to compute the  $N_{\text{res}}$  (`Nres`) eigenvalues the nearest to the numeric value  $\sigma = (2\pi/\lambda_t)^2$  (`sigma`). The `eigs` subroutine computes eigenvalues using a Krylov method [8] (MATLAB documentation on the algorithm used by the `eigs` subroutine is rather poor). If the expert mode is not activated in the WGRIN program, a default guess  $\lambda_t$  for the resonance wavelengths is provided. This default guess is  $\lambda_t = \frac{2\pi n_0 R}{q}$  where  $R$  is the radius of the cavity,  $n_0$  the refractive index at the cavity boundary and  $q$  the polar mode index. This guess is based on the first term of the asymptotic expansion for the resonances available for a micro-disk [9] and for a micro-sphere [10, 11]. Note that the eigenvalues computed by MATLAB `eigs` solver corresponds to  $k_q^2$ , see (17). The WGRIN program then deduces the corresponding values of the resonance wavenumbers  $k_q$  and resonance wavelengths  $\lambda_q = 2\pi/k_q$  and arranges the resonance wavelengths according to their distance to the guess value  $\lambda_t$ .

Even if the WGRIN program is provided with some default values for the PML parameters, the user can modify these values inside the WGRIN program. For convenience, an expert mode can be activated in the heading of the WGRIN program main file `wgrin.m` (by setting the variable `expert_mode` to 1) and the user will be asked by the WGRIN prompt in the MATLAB console to enter its own values for all the discretization parameters. Note that in the expert mode, an empty answer (carriage return) for any of the parameters will proceed to the computation with the default value. For the PML, these tunable parameters are:

- $R_1$  (variable `R1` in the program) that defines the location of the end boundary of the PML area (the condition  $R_1 > R$  must be fulfilled);
- $\sigma_0$  (variable `sigma0` in the program), the PML amplification parameter;
- $\aleph$  (variable `qpml` in the program) that tunes the regularity of the complex shift in coordinates.

Let us provide some criteria on how to choose the PML parameter values. We consider more specifically the case of a micro-disk but the same reasoning could be done in the case of a micro-sphere. The aim of the PML is to absorb the outgoing mode while preventing any reflection in the computational domain. In particular, it is wished that the mode  $u_q$  tends to zero at the PML end boundary  $R_1$  where a homogeneous Dirichlet boundary condition is imposed. One can show that the solution  $\tilde{u}_q$  to problem (5) is such that, in the PML area, we have

$$\frac{|u_q(R_1)|}{|u_q(R)|} \approx \left| \sqrt{\frac{R}{R_1(1+i\sigma_0)}} \right| \exp(-\text{Re}(k_q^{(j)})R_1\sigma_0)$$

since  $\tilde{\sigma}(R) = 0$  and  $\tilde{\sigma}(R_1) = \sigma_0$ . It follows that in order that  $\frac{|u_q(R_1)|}{|u_q(R)|} = 10^{-\alpha}$  with e.g.  $\alpha = 16$ ,

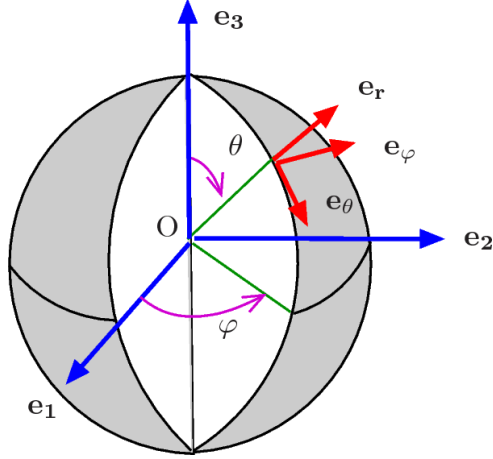


Figure 3: Spherical coordinates basis.

we must have

$$R_1\sigma_0 \approx \frac{\alpha \log(10)}{\operatorname{Re}(k_q^{(j)})}.$$

From asymptotic formulas for the resonances in a disk, see [12, 9], we have  $k_q^{(j)} \underset{m \rightarrow +\infty}{\sim} \frac{q}{n_0 R}$  where  $n_0 = N(R)$ . Thus,  $R_1\sigma_0$  must be chosen such that

$$R_1\sigma_0 \approx \frac{\alpha \log(10)n_0 R}{q}. \quad (20)$$

Default values for the PML parameters are:  $R_1 = 2R$  and  $\sigma_0 = \frac{16 \log(10)n_0 R}{qR_1}$ . We found that the value of the parameter  $\aleph$  has no real impact on the accuracy of the results and the default value is set to  $\aleph = 2$ . Other parameters in the WGRIN program that can be changed when the expert mode is activated, include the number of discretization nodes in the cavity (variable `Qi` in the program with default value  $10^4$  and denoted by  $J_R$  in Section 2) and the target wavelength  $\lambda_t$  (variable `lambdat` in the program with default value  $2\pi R n_0/q$ ).

The WGRIN program computes the resonances for the specified GRIN micro-cavity. It can also depict the corresponding modes associated to the computed resonances. The representation of the mode differs according to whether one considers a disk or a sphere cavity.

- For a TE mode in a micro-disk, the WGRIN program provides graphical representations of the radial variation of the modulus, real part and imaginary part of the magnetic field component  $H_z$  together with a bi-dimensional representation of the modulus, real part and imaginary part of  $H_z$ .
- For a TM mode in a micro-disk, the electric field component  $E_z$  is represented in a way similar to TE modes.
- For a TE mode in a micro-sphere, the WGRIN program provides graphical representations of the radial variation of the amplitude<sup>3</sup> of the electric field  $\mathbf{E} = \mathbf{M}_\ell^m$  and the amplitude of the magnetic field  $\mathbf{H} = -\frac{i}{\omega\mu_0} k N \mathbf{N}_\ell^m$ , see Appendix A, where  $\mathbf{M}_\ell^m$  and  $\mathbf{N}_\ell^m$  are the two Vector Harmonics functions defined in (A.17). It also provides a bi-dimensional representation of the amplitude of  $\mathbf{E}$  and  $\mathbf{H}$  in a azimuth plane  $\varphi = \text{cste}$  specified by the user and in a polar plane  $\theta = \text{cste}$  specified by the user, see Fig. 3. By default, these planes correspond to  $\varphi = 0$  and  $\theta = \frac{\pi}{2}$ .

<sup>3</sup>The amplitude of the electric field  $\mathbf{E}$  (resp. magnetic field  $\mathbf{H}$ ) is given by the euclidean norm of the real part of  $\mathbf{E}$  (resp.  $\mathbf{H}$ ).

- For a TM mode in a micro-sphere, the WGRIN program similarly provides the amplitude of the electric field  $\mathbf{E} = \mathbf{P}_\ell^m$  and the amplitude of the magnetic field  $\mathbf{H} = -\frac{i}{\omega\mu_0}\mathbf{M}_\ell^m$  where  $\mathbf{P}_\ell^m$  is defined in terms of  $u_\ell$  and the Spherical Surface Harmonics in (A.21).

Note that in all cases, the modes outside the cavity is computed from its values on the cavity boundary using respectively formula (7) in the case of a micro-disk and formula (9) in the case of a micro-sphere.

It should be noted that for  $\ell$  larger than 150, values of the associated Legendre function  $P_\ell^m$  involved in the definition of the Vector Harmonics  $\mathbf{M}_\ell^m$ ,  $\mathbf{N}_\ell^m$  and  $\mathbf{P}_\ell^m$ , are not anymore representable in the floating point arithmetic in MATLAB. As a consequence, we have used the Schmidt semi-normalized associated Legendre functions  $S_\ell^m$  instead of the associated Legendre functions  $P_\ell^m$  in the WGRIN toolbox to compute the electromagnetic field. They are related to each other by the relation [13]

$$P_\ell^m(x) = D_{\ell,m} S_\ell^m(x) \quad \text{where } D_{\ell,m} = \begin{cases} 1 & \text{if } m = 0 \\ (-1)^m \sqrt{(\ell+m)!/2(\ell-m)!} & \text{if } m > 0 \end{cases} \quad (21)$$

In terms of the Schmidt semi-normalized associated Legendre functions, we have

$$Y_\ell^m(\theta, \varphi) = K_{\ell,m} S_\ell^m(\cos(\theta)) e^{im\varphi} \quad \text{where } K_{\ell,m} = \begin{cases} \frac{2\ell+1}{4\pi} & \text{if } m = 0 \\ (-1)^m \frac{2\ell+1}{8\pi} & \text{if } m > 0 \end{cases} \quad (22)$$

The quality of the image display for modes can be adjusted in the expert mode of the WGRIN program. In the 2D mode rendering, a mesh-grid in the radial and angular directions is used to display the mode with a number of sampling points defined by the variables `nbpr` (number of point in the radial direction) and `nbpa` (number of point in the angular direction). By default these variables are set to the value 100. When the WGRIN program is run in the expert mode, it is possible to increase these values for a better rendering, for instance when the disk polar mode index is large. Note however that in this case, memory requirements are higher.

The mode displays can be automatically recorded in files in the raster-graphics file format PNG (Portable Network Graphics). The user is asked whether he wants the display of the graphical windows to be saved or not. If so, he is asked to provide the file prefix name (a character string) that will be supplemented by the number of the mode as it appears in the WGRIN table of results to distinguish between modes. The filename extension is “.png”.

### 3.3 A comprehensive test run for a micro-disk

We consider the case of a micro-disk with radius  $R = 10 \mu\text{m}$  and refractive index varying according to the radial position  $r$  as

$$n(r) = \frac{2n_0}{1+r^2/R^2} \quad \text{where } n_0 = n(R) = 1.45. \quad (23)$$

This refractive index profile corresponds to the modified form of “Maxwell’s fish eye” GRIN studied in [14]. Its value is 1 outside the cavity.

The first step for computing the resonances of this dielectric cavity is to provide the refractive index function in the file named `optindex.m`. For this particular example, the file must be as follows:

```
% Definition of the refractive index N
% Some useful variables defined in the main program are:
% R is the radius of the cavity
% n0 is the refractive index value at the cavity boundary
N=@(r) 2*n0./(1+(r./R).^2).*(r<=R)+(r>R);
```

Note that the variation of the refractive index will be depicted by the WGRIN program, see Fig. 4.

Then, running the `wgrin` program, the user provides the characteristics of the cavity (disk or sphere, radius  $R$  and value  $n_0$  of the refractive index  $N$  at the cavity boundary), the characteristics of the modes (TE or TM modes), the polar mode index  $q$  (also denoted  $m$  for a disk and  $\ell$  for a sphere) and the number of modes to be computed. If the expert mode is activated (by setting the variable `expert_mode` to 1 in the `wgrin` program) then the user is also asked to provide the target value of the resonance wavelength, the number of discretization nodes inside the cavity for the Finite Difference scheme and the PML parameters: position  $R_1$  of the PML outer side, PML amplification coefficient  $\sigma_0$  and PML regularity parameter  $\aleph$ .

We provide below an example of execution of the `wgrin` program in the basic mode to compute TE modes in a micro-disk and then an execution for the same micro-disk in the expert mode with different PML parameters. Computations were performed on an Intel Core i5 processor with 8 GO RAM.

```
>> wgrin
[?] Geometry : sphere (0) or disk (1) : ans = 1
[?] Radius in mu-m: R = 10
[?] Optical index at the boundary: n0 = 1.45
[?] Polar mode index: m = 60
[?] TE or TM mode : TE
[*] TE modes
[?] Number of resonances to compute = 5
[*] PML parameters : R1 = 20, sigma0 = 0.44517, qpml = 2

[*] Computation of the FDM matrices
[*] Solving the generalized eigenvalue problem
[*] CPU time for the computations (sec.): 72.4

Wavenumber #1 = 4.235543978990459-4.19432897415177e-12i mu-m^(-1)
Wavelength #1 = 1.483442348455364+1.469007346983824e-12i mu-m

Wavenumber #2 = 4.369633740207968-9.573664704954836e-11i mu-m^(-1)
Wavelength #2 = 1.437920356885688+3.150416759780281e-11i mu-m

Wavenumber #3 = 4.504389754715657-1.423331090603349e-09i mu-m^(-1)
Wavelength #3 = 1.394902672576614+4.407718804007733e-10i mu-m

Wavenumber #4 = 4.639383995299243-1.665431052923363e-08i mu-m^(-1)
Wavelength #4 = 1.354314562783743+4.861674589927731e-09i mu-m

Wavenumber #5 = 4.774434864118084-1.594548735427607e-07i mu-m^(-1)
Wavelength #5 = 1.316006079463016+4.395150189592987e-08i mu-m
```

Since spurious resonances may be intruded among the computed resonances, one may want the WGRIN program to detect WGM resonances. This is achieved by comparing the MATLAB 2-norm of the associated mode inside and outside the cavity. WGM are located inside the cavity whereas spurious modes introduced by the numerical discretization are located in the PML area. Note that this approach do not distinguish between spurious resonances and outer resonances, see Section 3.5 for details.

```

[?] Auto-detection of spurious modes (y/n) ? ans = y
[*] The resonances identified as WGM are :
Wavenumber #1 = 4.235543978990459-4.19432897415177e-12i mu-m^(-1)
Wavelength #1 = 1.483442348455364+1.469007346983824e-12i mu-m

Wavenumber #2 = 4.369633740207968-9.573664704954836e-11i mu-m^(-1)
Wavelength #2 = 1.437920356885688+3.150416759780281e-11i mu-m

Wavenumber #3 = 4.504389754715657-1.423331090603349e-09i mu-m^(-1)
Wavelength #3 = 1.394902672576614+4.407718804007733e-10i mu-m

Wavenumber #4 = 4.639383995299243-1.665431052923363e-08i mu-m^(-1)
Wavelength #4 = 1.354314562783743+4.861674589927731e-09i mu-m

Wavenumber #5 = 4.774434864118084-1.594548735427607e-07i mu-m^(-1)
Wavelength #5 = 1.316006079463016+4.395150189592987e-08i mu-m

```

It is also possible to visualize some of the computed modes. The user must provide the value  $R_o$  of the radial position of the outer boundary up to which the mode in the exterior domain must be displayed and he then successively provides the index of the modes he wants a display. For each of the specified mode, a MATLAB figure windows is open for graphical display of the modes. For a micro-disk, each figure window is shared into six subplots. The first column corresponds to the radial variation of the modulus, the real part and the imaginary part of the mode  $u_m$  along the interval  $[0, R_o]$  where  $u_m$  denotes the approximated solution to problem (1). The position of the disk boundary is marked with a black line. The second column provides the modulus, the real part and the imaginary part of the bi-dimensional representation of the mode corresponding to the function  $(r, \theta) \in [0, R_o] \times [0, 2\pi] \mapsto u_m(r)e^{im\theta}$ . The position of the disk boundary is marked with a black circle. We show in Fig. 5 and in Fig. 6 the representation of the modes corresponding to the first resonance and to the third resonance of the previous execution of the WGRIN program. The modes are represented in arbitrarily unit since they are defined up to a multiplicative complex valued constant. In the WGRIN toolbox a mode is normalized such that its maximum value is 1. The user is successively asked for the index of the resonances for which the modes must be displayed. He is also asked whether the figures have to be saved or not. If so, he must provide the prefix of the files name; Each mode is saved in the PNG format (Portable Network Graphics format) in a file formed by the prefix provided by the user complemented by the resonance reference number and the extension `.png`. Note that in the expert mode, the user is asked to provide the number of sampling points in the radial and angular directions for the display of the modes. This can be useful, e.g. to improve the quality of the image by increasing the number of sampling points; However, time for the display and memory requirements also increase in this case.

```

[?] Graphical display of the modes (y/n) ? ans = y
[?] Value of the external boundary untill where the mode is displayed = 1.5*R
[?] Name of the figures backup files (if empty, no backup) : disk_fisheye
[?] Index of the computed modes to be displayed = 1
[?] Display another mode (y/n) ? ans = : y
[?] Index of the computed modes to be displayed = 3
[?] Display another mode (y/n) ? ans = : n

```

Under the expert mode, computation of TE modes with the same micro-disk as in the previous run, is obtained as follows.

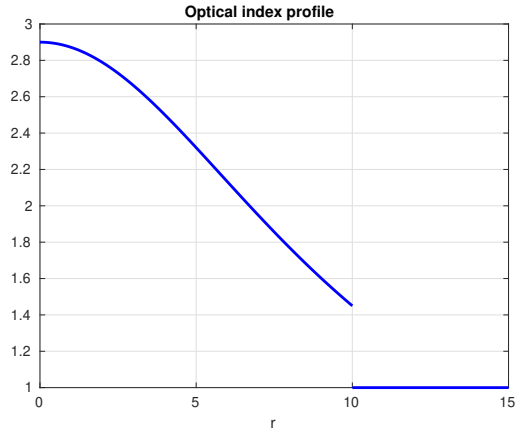


Figure 4: Figure window of the refractive index profile provided by the `wgrin` program.

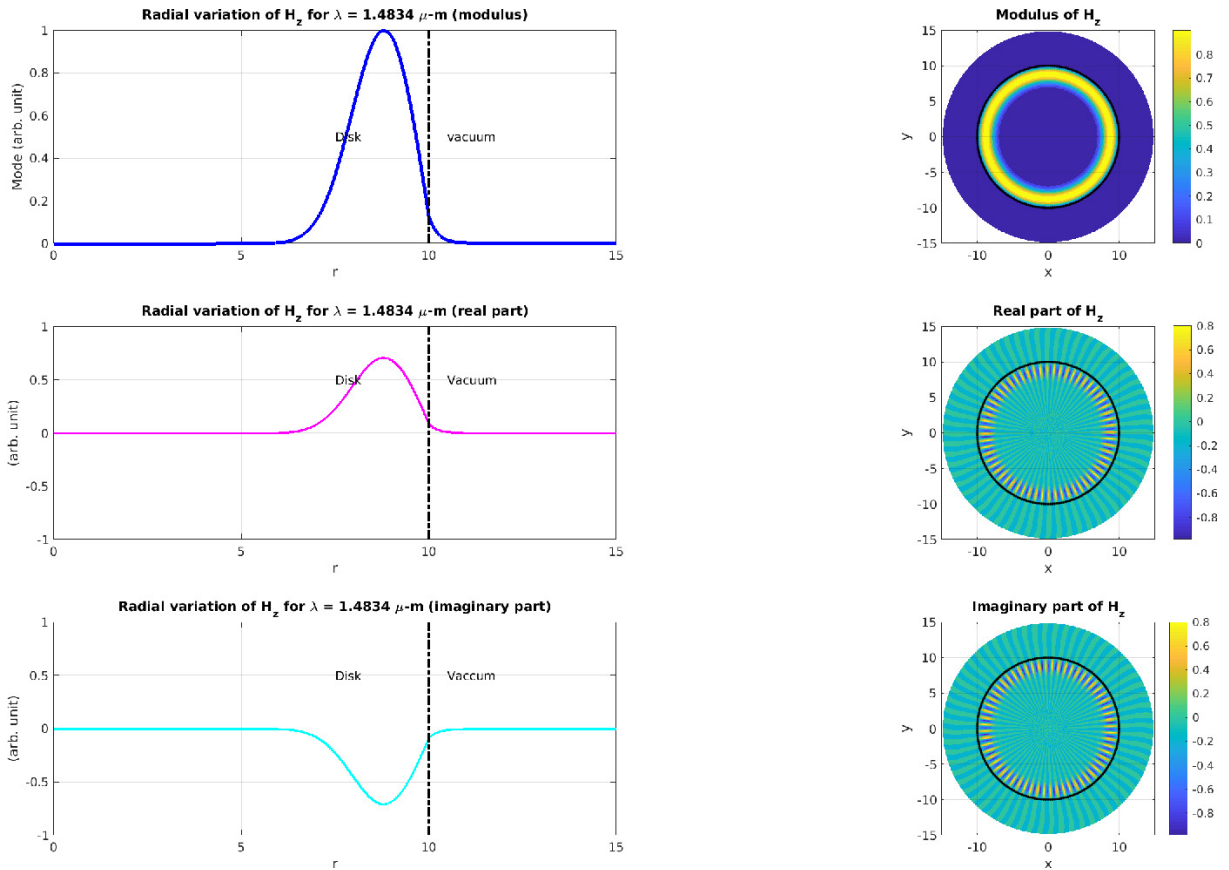


Figure 5: WGRIN representation of the mode corresponding to the first resonance of the disk with radius  $R = 10 \mu\text{m}$  and radially varying refractive index defined in (23). The first column shows the radial variation of the magnetic field component  $H_z$ : from top to bottom, the modulus, the real part and the imaginary part of  $H_z$ . The second column shows the bi-dimensional variation of the magnetic field component  $H_z$ : from top to bottom, the modulus, the real part and the imaginary part of  $H_z$ .

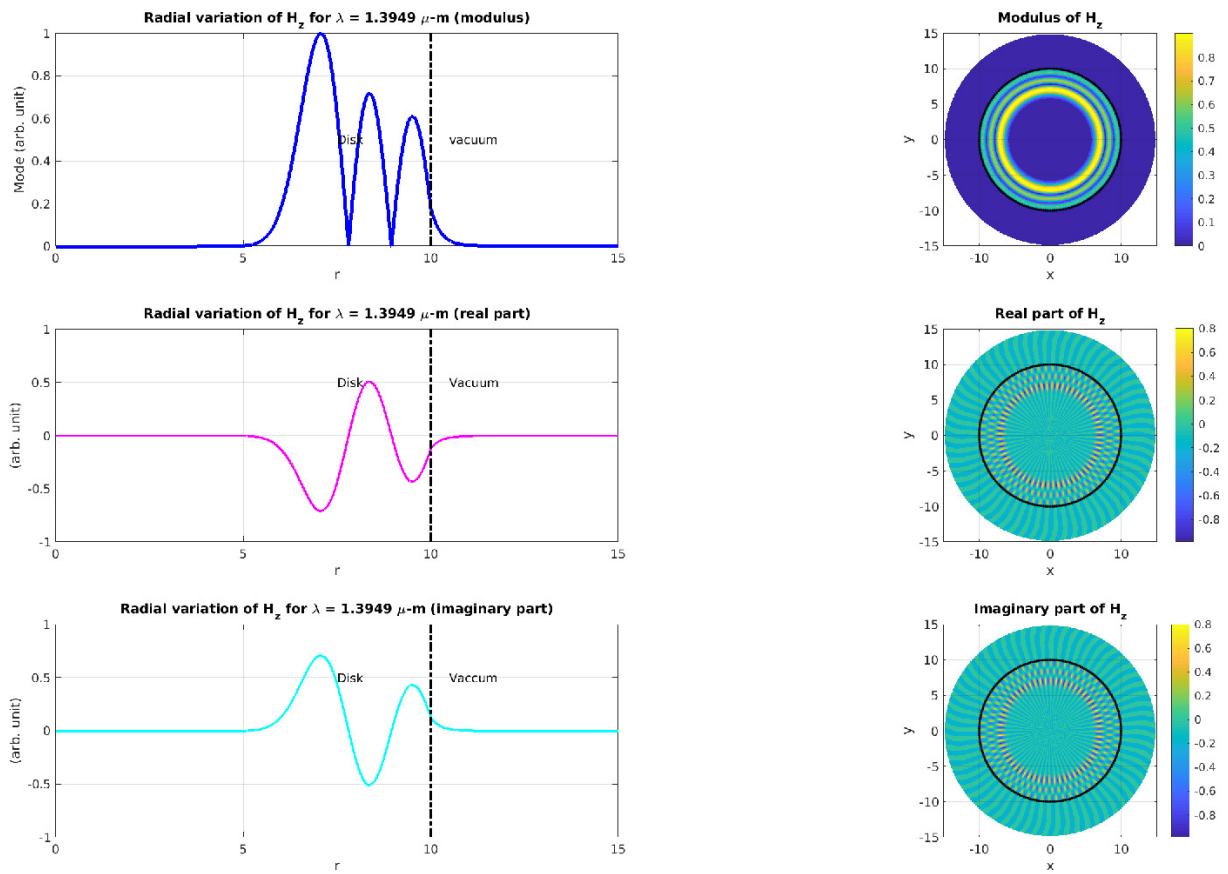


Figure 6: WGRIN representation of the mode corresponding to the third resonance of the disk with radius  $R = 10 \mu\text{m}$  and radially varying refractive index defined in (23).

```

>> wgrin
[?] Geometry : sphere (0) or disk (1) : ans = 1
[?] Radius in mu-m: R = 10
[?] Optical index at the boundary: n0 = 1.45
[?] Polar mode index: m = 60
[?] TE or TM mode : TE
[*] TE modes
[?] Number of resonances to compute = 5
[?] Target resonance wavelength in mu-m : lambda = 1.5
[?] Number of discretization sub-intervals inside the cavity: Qi = 1E4
[*] Step-size of the FDM = 0.001
[?] PML outer boundary position = 1.5*R
[?] PML parameter sigma0 = 1
[?] PML regularity = 2
[*] PML parameters : R1 = 15, sigma0 = 1, qpml = 2

[*] Computation of the FDM matrices
[*] Solving the generalized eigenvalue problem
[*] CPU time for the computations (sec.): 54.39

Wavenumber #1 = 4.235543978990701+2.283822661974355e-12i mu-m^(-1)
Wavelength #1 = 1.48344234845528-7.998781903669295e-13i mu-m

Wavenumber #2 = 4.369633740208481-8.405479665891252e-11i mu-m^(-1)
Wavelength #2 = 1.43792035688552+2.766000777080156e-11i mu-m

Wavenumber #3 = 4.504389754716508-1.405907838095475e-09i mu-m^(-1)
Wavelength #3 = 1.39490267257635+4.353763123410803e-10i mu-m

Wavenumber #4 = 4.639383995300634-1.663014863934398e-08i mu-m^(-1)
Wavelength #4 = 1.354314562783336+4.854621326091715e-09i mu-m

Wavenumber #5 = 4.774434864120844-1.594228227396461e-07i mu-m^(-1)
Wavelength #5 = 1.316006079462256+4.394266754103896e-08i mu-m

[?] Auto-detection of spurious modes (y/n) ? ans = n
[?] Graphical display of the modes (y/n) ? ans = n

```

One can note that the resonance values have not significantly changed in this run with some new PML parameters. For instance, there are 8 digits in common on the real part of the first computed resonance wavelength. (Note that the imaginary parts significantly differ in the two computations; This can be related to the fact that the imaginary part in this particular example is below the numerical error.) The fact that the resonance values do not significantly change with a change in the PML parameters indicates, as detailed in Section 3.5, that the above computed resonances are not spurious resonances.

### 3.4 A comprehensive test run for a micro-sphere

We consider the case of a micro-sphere with radius  $R = 500 \mu\text{m}$  and refractive index varying according to the radial position  $r$  as  $n(r) = n_0 \sqrt{1 + \epsilon'(R - r)}$  where  $\epsilon' = 4 \cdot 10^{-3} \mu\text{m}^{-1}$  and  $n_0 = n(R) = 1.45$ . Such a refractive index profile is investigated in [11]. The value is 1 outside the cavity.

The first step for computing the resonances of this dielectric cavity is to provide the refractive index function in the file named `optindex.m`. For this particular example, the file must be as follows:

```
% Definition of the refractive index N and expression of its derivative dN
% Some useful variables defined in the main program are:
% R is the radius of the cavity
% n0 is the refractive index value at the cavity boundary
eps=4E-3;
N=@(r) n0*sqrt(1+(eps/n0^2)*(R-r)).*(r<=R)+(r>R);
```

Using the `WGRIN` program in the expert mode, the first five resonances corresponding to a polar mode index  $\ell = 3000$  are obtained as illustrated below.

```
>> wgrin
[?] Geometry : sphere (0) or disk (1) : ans = 0
[?] Radius in mu-m: R = 500
[?] Optical index at the boundary: n0 = 1.45
[?] Polar mode index: ell = 3E3
[?] TE or TM mode : TE
[*] TE modes
[?] Number of resonances to compute = 5
[?] Target resonance wavelength in mu-m : lambda = 1.55
[?] Number of discretization sub-intervals inside the cavity: Qi = 1E4
[*] Step-size of the FDM = 0.05
[?] PML outer boundary position = 1.5*R
[?] PML parameter sigma0 = 0.5
[?] PML regularity = 2
[*] PML parameters : R1 = 750, sigma0 = 0.5, qpml = 2

[*] Computation of the FDM matrices
[*] Solving the generalized eigenvalue problem
[*] CPU time for the computations (sec.): 34.83

Wavenumber #1 = 4.14214533888064-7.258262874179645e-17i mu-m^(-1)
Wavelength #1 = 1.516891560564491+2.658042342178407e-17i mu-m

Wavenumber #2 = 4.14677546565527-1.025334297156278e-16i mu-m^(-1)
Wavelength #2 = 1.515197858967443+3.746487709894812e-17i mu-m

Wavenumber #3 = 4.151356330683101-1.180821678705239e-16i mu-m^(-1)
Wavelength #3 = 1.513525895317614+4.305109092330583e-17i mu-m

Wavenumber #4 = 4.155899669044884-1.516371281094346e-16i mu-m^(-1)
Wavelength #4 = 1.511871269169402+5.516394417209356e-17i mu-m

Wavenumber #5 = 4.160411798907187-1.195507411074092e-16i mu-m^(-1)
Wavelength #5 = 1.51023158544786+4.339697943639473e-17i mu-m

[?] Auto-detection of spurious modes (y/n) ? ans = y
[*] The resonances identified as WGM are :
Wavenumber #1 = 4.14214533888064-7.258262874179645e-17i mu-m^(-1)
Wavelength #1 = 1.516891560564491+2.658042342178407e-17i mu-m
```

```

Wavenumber #2 = 4.14677546565527-1.025334297156278e-16i mu-m^(-1)
Wavelength #2 = 1.515197858967443+3.746487709894812e-17i mu-m

Wavenumber #3 = 4.151356330683101-1.180821678705239e-16i mu-m^(-1)
Wavelength #3 = 1.513525895317614+4.305109092330583e-17i mu-m

Wavenumber #4 = 4.155899669044884-1.516371281094346e-16i mu-m^(-1)
Wavelength #4 = 1.511871269169402+5.516394417209356e-17i mu-m

Wavenumber #5 = 4.160411798907187-1.195507411074092e-16i mu-m^(-1)
Wavelength #5 = 1.51023158544786+4.339697943639473e-17i mu-m

```

The graphical representation of the refractive index provided by the WGRIN program is given in Fig. 7.

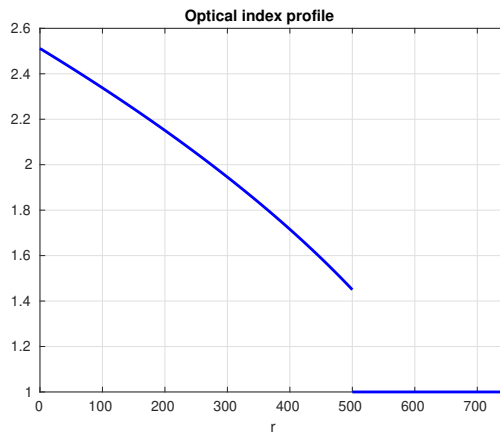


Figure 7: Figure window of the refractive index profile provided by the wgrin program.

It is also possible to visualize some of the modes.

```

[?] Graphical display of the modes (y/n) ? ans = y
[?] Value of the external boundary untill where the mode is displayed = 1.1*R
Image display quality
[?] Number of sampling points in the 2 angular directions = 300
[?] Number of sampling points in the radial direction = 200
[?] Azimuthal mode number m = ell-2
Name of the figures backup files (if empty, no backup) :
[?] Azimuthal angle [radian] : phi = 0
[?] Polar angle [radian] : theta = pi/2
[?] Index of the computed modes to be displayed = 1
[?] Display a mode for an other radial mode index n (y/n) ? ans = : n
[?] Display a mode for an other azimuthal mode index m (y/n) ? ans = : n

```

We have depicted in Fig. 8 the mode with polar mode index  $\ell = 3000$  and azimuthal mode index  $m = 2998$  corresponding to the first resonance (radial mode index  $j = 1$ ) as provided by the WGRIN program. The graphical representations of the mode provided by the WGRIN program are not clearly legible in this particular test case due to the fact that quality factor of this resonator is high. However, using MATLAB tools available in the graphical windows, one

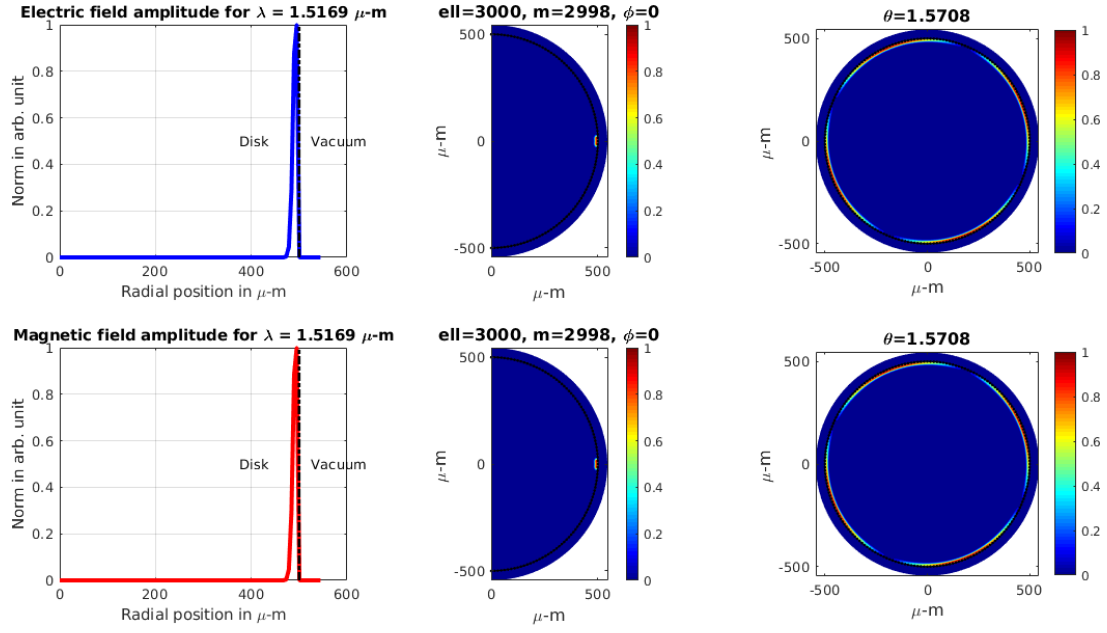


Figure 8: WGRIN representation of the mode with polar mode index  $\ell = 3000$ , azimuthal mode index  $m = 2998$  and radial mode index  $n = 1$ . The first column corresponds to the radial variation of the amplitude of the electric field  $\mathbf{E}$  and the amplitude of the magnetic field  $\mathbf{H}$ . The second column corresponds to a bi-dimensional representation of the amplitude of  $\mathbf{E}$  and  $\mathbf{H}$  in an azimuth plane  $\varphi = 0$ . The third column corresponds to a bi-dimensional representation of the amplitude of  $\mathbf{E}$  and  $\mathbf{H}$  in a polar plane  $\theta = \frac{\pi}{2}$ .

can easily enlarge the display in the vicinity of the cavity boundary to make the figure clearer as illustrated in Fig. 9.

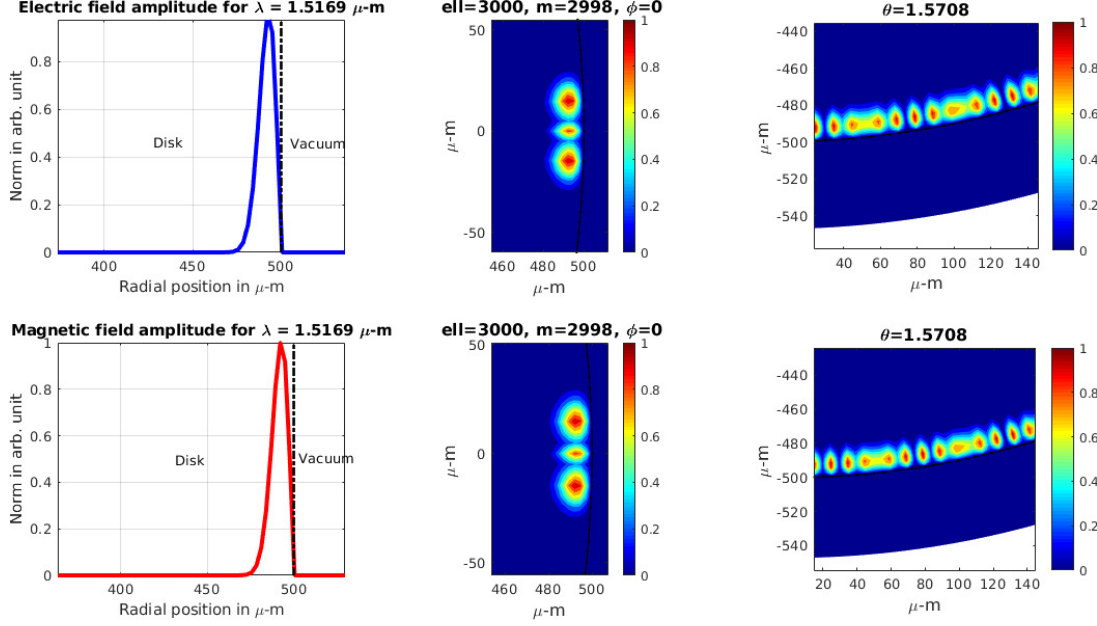


Figure 9: WGRIN representation of the mode with polar mode index  $\ell = 3000$ , azimuthal mode index  $m = 2998$  and radial mode index  $n = 1$ . This figure corresponds to an enlargement in the vicinity of the cavity boundary of the mode depicted in Fig. 8 using MATLAB graphical tools.

### 3.5 Detection of spurious resonances

Spurious resonances, that is to say computed resonances without any physical meaning, are inherent to the discretization of the resonance problem (1). The use of a PML to bound the computational domain rather than a Dirichlet boundary condition (perfect electric/magnetic wall condition) [15, 4, 16] reduces the number of spurious resonances in the vicinity of the look after resonances and above all it allows an approximation of the imaginary part of the resonances which is not possible when using a Dirichlet boundary condition (the eigenvalues are then real). However, it may sometimes remains some spurious resonances among the  $N_{\text{Res}}$  resonances computed by the WGRIN program and this number may vary depending on the PML parameters values. The questions are then :

- How to know if a computed resonance is a spurious resonance or a physical resonance?
- What is the impact of the PML parameters values on the number of spurious resonances among the computed resonances?

There exist some simple criteria to decide whether a resonance is of Whispering Gallery Mode (WGM) type or not. The first one is that WGM resonances, that are actually the resonance of primary importance in the study of optical micro-resonators, have a very small imaginary part. The imaginary part of the resonance takes into account the mode leakage and the smaller is the imaginary part, the higher is the micro-resonator quality factor. However, it can be sometime difficult to decide whether the imaginary part of a resonance has to be consider small or not. Therefore, in the WGRIN program an other criterion is used. The MATLAB 2-norm of the computed eigenvector inside and outside the cavity are computed and their values compared. WGM are localized inside the dielectric cavity, in the vicinity of the cavity boundary, whereas spurious resonances related to the discretization are localized inside the PML. It is thus easy to filter WGM resonances automatically at a low computational cost.

The main drawback of these easy-to-use and computational cheap methods is that they do not distinguish between spurious resonances and outer resonances (*i.e.* resonances for which

the mode is located outside the cavity) [17]. So, when outer resonances are expected, one should distinguish them from spurious modes in an other way, for instance using the approach described in [7] where a general and reliable criteria has been identified. The method consists in changing the PML parameters and observing if a resonance value is shifted or not by this change. The resonance that are not shifted are the physical resonances whereas the values that change with a change in the discretization parameters correspond to spurious resonances related to the discretization.

In order to illustrate this point, let us consider the micro-sphere with radius  $R = 10 \mu\text{m}$  and constant optical index  $N = n_0 = 1.45$ . We are looking for the resonances corresponding to TE modes with polar mode index  $\ell = 60$ .

```
>> wgrin
[?] Geometry : sphere (0) or disk (1) : ans = 0
[?] Radius in mu-m: R = 10
[?] Optical index at the boundary: n0 = 1.45
[?] Polar mode index: ell = 60
[?] TE or TM mode : TE
[*] TE modes
[?] Number of resonances to compute = 20
[*] PML parameters : R1 = 20, sigma0 = 0.4415, qpml = 2

[*] Computation of the FDM matrices
[*] Solving the generalized eigenvalue problem
[*] CPU time for the computations (sec.): 42.98

Wavenumber #1 = 4.588033246292139-1.73396316455934e-08i mu-m^(-1)
Wavelength #1 = 1.369472488512894+5.175670537866828e-09i mu-m

Wavenumber #2 = 4.993674552899072-7.067196909528906e-06i mu-m^(-1)
Wavelength #2 = 1.258228833418731+1.780682907710654e-06i mu-m

Wavenumber #3 = 5.338411612710144-0.0003504458750686014i mu-m^(-1)
Wavelength #3 = 1.17697654956827+7.726391420748446e-05i mu-m

Wavenumber #4 = 5.650863394760268-0.003979956466311404i mu-m^(-1)
Wavelength #4 = 1.111897731631917+0.0007831200752417359i mu-m

Wavenumber #5 = 5.67424549190582-0.7041785208049409i mu-m^(-1)
Wavelength #5 = 1.090521304655885+0.135334588592312i mu-m

Wavenumber #6 = 5.947343139611172-0.01400180736026578i mu-m^(-1)
Wavelength #6 = 1.056463421396866+0.002487227819603042i mu-m

Wavenumber #7 = 5.377900045247969-1.128823266236945i mu-m^(-1)
Wavelength #7 = 1.119031846283636+0.2348852104198617i mu-m

Wavenumber #8 = 5.124066330206219-1.456371272620318i mu-m^(-1)
Wavelength #8 = 1.13455881209127+0.3224663293852132i mu-m

Wavenumber #9 = 4.891014078864517-1.730853406721978i mu-m^(-1)
Wavelength #9 = 1.141663335385394+0.4040168033701797i mu-m

Wavenumber #10 = 4.672681946446131-1.968882408085997i mu-m^(-1)
Wavelength #10 = 1.141921724494184+0.4811604171941994i mu-m

Wavenumber #11 = 4.207979950209577-1.85783394314159i mu-m^(-1)
Wavelength #11 = 1.249584804123375+0.5516948966970998i mu-m
```

Wavenumber #12 = 4.041476238831348-1.784322396836121i  $\mu\text{-m}^{-1}$   
Wavelength #12 = 1.301066054103875+0.5744240873656707i  $\mu\text{-m}$

[The other resonances values are not provided for the sake of conciseness.]

[?] Auto-detection of spurious modes (y/n) ? ans = y

[\*] The resonances identified as WGM are :

Wavenumber #1 = 4.588033246292139-1.73396316455934e-08i  $\mu\text{-m}^{-1}$

Wavelength #1 = 1.369472488512894+5.175670537866828e-09i  $\mu\text{-m}$

Wavenumber #2 = 4.993674552899072-7.067196909528906e-06i  $\mu\text{-m}^{-1}$

Wavelength #2 = 1.258228833418731+1.780682907710654e-06i  $\mu\text{-m}$

Wavenumber #3 = 5.338411612710144-0.0003504458750686014i  $\mu\text{-m}^{-1}$

Wavelength #3 = 1.17697654956827+7.726391420748446e-05i  $\mu\text{-m}$

Wavenumber #4 = 5.650863394760268-0.003979956466311404i  $\mu\text{-m}^{-1}$

Wavelength #4 = 1.111897731631917+0.0007831200752417359i  $\mu\text{-m}$

Wavenumber #6 = 5.947343139611172-0.01400180736026578i  $\mu\text{-m}^{-1}$

Wavelength #6 = 1.056463421396866+0.002487227819603042i  $\mu\text{-m}$

[?] Graphical display of the modes (y/n) ? ans = n

The WGRIN program has identified five resonances as WGM resonances among the twenty resonances computed. Using the program `rspurious` provided in the WGRIN toolbox, one can compare the behavior of the mode  $u_q = S_\ell$  solution to problem (1) for the various computed resonances.

>> `rspurious`

[?] Index of the computed modes to be displayed = 4

[?] Display another mode (y/n) ? ans = : y

[?] Index of the computed modes to be displayed = 5

[?] Display another mode (y/n) ? ans = : n

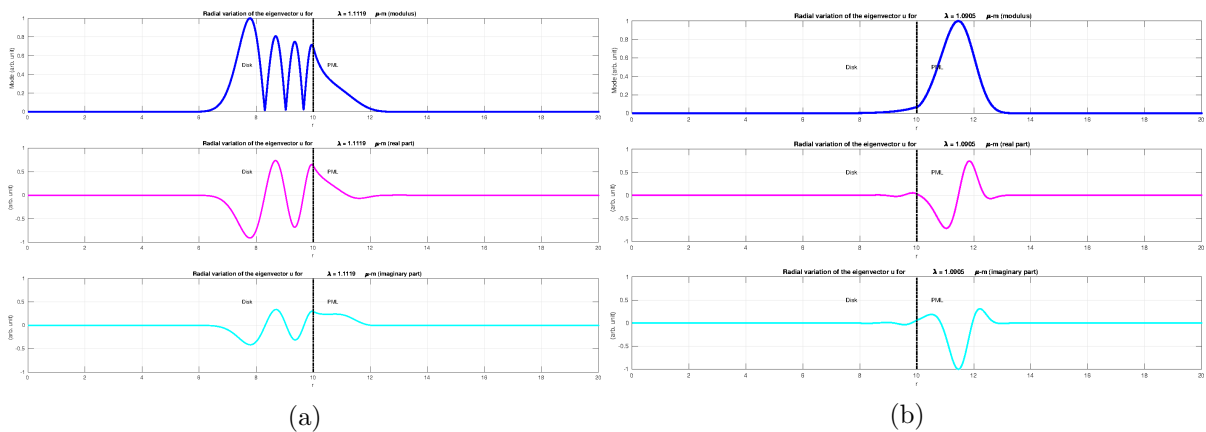


Figure 10: Mode  $u_q = S_\ell$  solution to problem (1) for the fourth (a) and fifth (b) computed resonances.

We have depicted in Fig. 10 the mode  $u_q = S_\ell$  solution to problem (1) for the fourth (a) and fifth (b) computed resonances. The fourth one is of WGM type and the mode is located in the dielectric cavity. One can also identify that the radial mode index for this resonance is  $j = 4$ :

the modulus of  $u_q$  has four local maxima inside the cavity. Note that in the PML area this is not the mode  $u_q$  that is depicted but the mode under the coordinate stretching, that is to say  $\tilde{u}_q$  with the notation introduced in Section 1.2. One can observe that the PML fulfilled its role: the mode outside the cavity is absorbed by the PML without any reflection in the cavity. The fifth resonance is not of WGM type since the mode is located outside the dielectric cavity. It can be either an outer resonance or a spurious resonance.

In order to identify the type of the fifth resonance (outer resonance or spurious resonance), we use the approach described in [7] that consists in a second execution with new PML parameters. If the fifth resonance value is shifted by this change of the discretization parameters, this will indicate that it is a spurious resonance. On the contrary, if the fifth resonance value remains unchanged (up to the computational accuracy) this will show that it is an outer resonance.

```
>> wgrin
[?] Geometry : sphere (0) or disk (1) : ans = 0
[?] Radius in mu-m: R = 10
[?] Optical index at the boundary: n0 = 1.45
[?] Polar mode index: ell = 60
[?] TE or TM mode : TE
[*] TE modes
[?] Number of resonances to compute = 20
[?] Target resonance wavelength in mu-m : lambda = 1.4
[?] Number of discretization sub-intervals inside the cavity: Qi = 1E4
[*] Step-size of the FDM = 0.001
[?] PML outer boundary position = 2*R
[?] PML parameter sigma0 = 1
[?] PML regularity = 2
[*] PML parameters : R1 = 20, sigma0 = 1, qpml = 2

[*] Computation of the FDM matrices
[*] Solving the generalized eigenvalue problem
[*] CPU time for the computations (sec.): 44.32

Wavenumber #1 = 4.588033246302807-1.732415768625441e-08i mu-m^(-1)
Wavelength #1 = 1.36947248850971+5.171051747946207e-09i mu-m

Wavenumber #2 = 4.993674552911803-7.067179371720165e-06i mu-m^(-1)
Wavelength #2 = 1.258228833415523+1.780678488795937e-06i mu-m

Wavenumber #3 = 5.338411612730631-0.0003504458351444487i mu-m^(-1)
Wavelength #3 = 1.176976549563754+7.726390540468686e-05i mu-m

Wavenumber #4 = 5.650863394719128-0.003979956399148256i mu-m^(-1)
Wavelength #4 = 1.111897731640031+0.0007831200620377285i mu-m

Wavenumber #5 = 5.674245476260446-0.704178511034266i mu-m^(-1)
Wavelength #5 = 1.090521308030529+0.1353345875064554i mu-m

Wavenumber #6 = 5.947343139542304-0.0140018073699966i mu-m^(-1)
Wavelength #6 = 1.056463421409091+0.00248722782138917i mu-m

Wavenumber #7 = 5.377899980543093-1.128823198748748i mu-m^(-1)
Wavelength #7 = 1.119031864257551+0.2348852029757196i mu-m

Wavenumber #8 = 6.237542250106264-0.02460767420896846i mu-m^(-1)
Wavelength #8 = 1.007301797225336+0.003973897644670414i mu-m

Wavenumber #9 = 5.124066299947559-1.456371088852832i mu-m^(-1)
```

```

Wavelength #9 = 1.134558839190339+0.3224662983022196i mu-m

Wavenumber #10 = 6.521228368764321-0.0321075598875408i mu-m^(-1)
Wavelength #10 = 0.9634738492565768+0.004743706640187283i mu-m

Wavenumber #11 = 4.891015995724708-1.730852514760547i mu-m^(-1)
Wavelength #11 = 1.141663118504647+0.4040163600774204i mu-m

Wavenumber #12 = 4.670737168546394-1.969544899442375i mu-m^(-1)
Wavelength #12 = 1.142137753590133+0.4816138236577537i mu-m

Wavenumber #13 = 4.459262018127697-2.181502027992055i mu-m^(-1)
Wavelength #13 = 1.136926027216357+0.5561921286452673i mu-m

Wavenumber #14 = 4.2542904580112-2.372205616899279i mu-m^(-1)
Wavelength #14 = 1.126616564061441+0.628204906960605i mu-m

Wavenumber #15 = 2.31241876379066-2.312419437404983i mu-m^(-1)
Wavelength #15 = 1.358573882736076+1.358574278492606i mu-m

Wavenumber #16 = 2.206698605662269-2.206699026508928i mu-m^(-1)
Wavelength #16 = 1.423661594014404+1.423661865525531i mu-m

Wavenumber #17 = 2.096259504480139-2.096259740942331i mu-m^(-1)
Wavelength #17 = 1.498665738901962+1.498665907954402i mu-m

Wavenumber #18 = 1.979046909029419-1.979047021140842i mu-m^(-1)
Wavelength #18 = 1.587426988863956+1.587427078790423i mu-m

Wavenumber #19 = 1.850991812678877-1.85099185167617i mu-m^(-1)
Wavelength #19 = 1.69724823517992+1.697248270938094i mu-m

Wavenumber #20 = 1.701204571165077-1.701204578069632i mu-m^(-1)
Wavelength #20 = 1.846687161607911+1.846687169102925i mu-m

[?] Auto-detection of spurious modes (y/n) ? ans = n
[?] Graphical display of the modes (y/n) ? ans = n

```

We can conclude that the resonance number 5 is not a spurious resonances but an outer resonance. Its value has not significantly changed with the change of the PLM parameter. One can also note that the resonance with number 11 in the first computation ( $k = 4.207979950209577 - i1.85783394314159 \mu\text{m}^{-1}$ ) is not found in this second computation. It is therefore a spurious resonance.

It can be useful to have a wider view of the spectrum of the Finite Difference matrix  $C^{-1}A$  to identify the spurious resonances. This can be obtained easily with the WGRIN toolbox in two steps. The first step consists in a first computation of the resonances. Let us consider the previous example of the micro-sphere where 200 resonances are computed by the WGRIN program.

```

>> wgrin
[?] Geometry : sphere (0) or disk (1) : ans = 0
[?] Radius in mu-m: R = 10
[?] Optical index at the boundary: n0 = 1.45
[?] Polar mode index: ell = 60
[?] TE or TM mode : TE
[*] TE modes
[?] Number of resonances to compute = 200

```

```
[*] PML parameters : R1 = 20, sigma0 = 0.4415, qpml = 2
```

```
[*] Computation of the FDM matrices  
[*] Solving the generalized eigenvalue problem  
[*] CPU time for the computations (sec.): 61.85
```

```
Wavenumber #1 = 4.588033246292139-1.733963161272877e-08i mu-m^(-1)
```

```
Wavelength #1 = 1.369472488512894+5.175670528057133e-09i mu-m
```

```
[The other resonances values are not provided for the sake of conciseness.]
```

```
[?] Auto-detection of spurious modes (y/n) ? ans = n
```

```
[?] Graphical display of the modes (y/n) ? ans = n
```

In a second step, using the program entitled `rspectrum` in the `WGRIN` toolbox, a second computation is achieved where one of the PML parameter can be changed: the location of the PML end  $R_1$ , the PML amplification coefficient  $\sigma_0$  or the PML regularity parameter  $\aleph$ . Once these new computation is achieved, the spectrum of the finite Difference matrix  $C^{-1}A$  in the two cases is depicted. The eigenvalues of the matrix are represented by a mark in the complex plane and the kind of mark and its color are different in the two executions. As mentioned before, when two marks are superimposed at the same location, it means that this eigenvalue corresponds to a true resonance (either a WGM or an outer resonance). On the contrary, when a mark is alone, it corresponds to a spurious resonance. Instead of displaying the spectrum of the finite Difference matrix  $C^{-1}A$  with eigenvalues  $k_q^2$ , for an easier analysis of the results, the `rspectrum` program displays, in the complex plane, the values of the resonance wavenumbers  $k_q$  and the values of the resonance wavelengths  $\lambda_q = 2\pi/k_q$  in two separated graphic windows.

```
>> rspectrum
```

```
[?] Select the PML parameter to modify :
```

```
(1) R1 (2) sigma0 (3) qpml : rep = 2
```

```
[?] New value of the PML amplification coefficient : sigma0 = 1
```

```
[*] PML parameters : R1 = 20, sigma0 = 1, qpml = 2
```

```
[*] Computation of the FDM matrices for the new set of PML parameters
```

```
[*] Solving the generalized eigenvalue problem
```

```
[?] Modify another PML parameter (y/n) ? ans = : n
```

```
>> figure(2)
```

```
>> xlim([2,10])
```

```
>> ylim([-8,0])
```

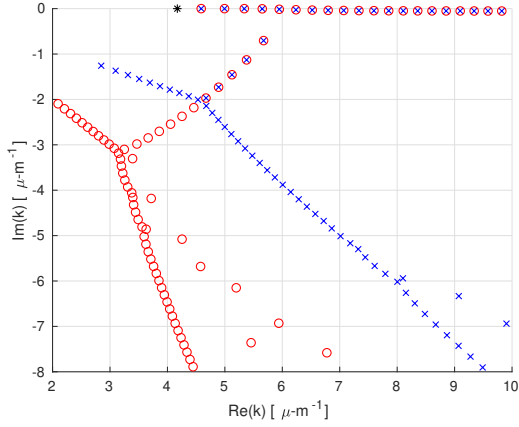
```
>> figure(3)
```

```
>> xlim([0.3,1.6])
```

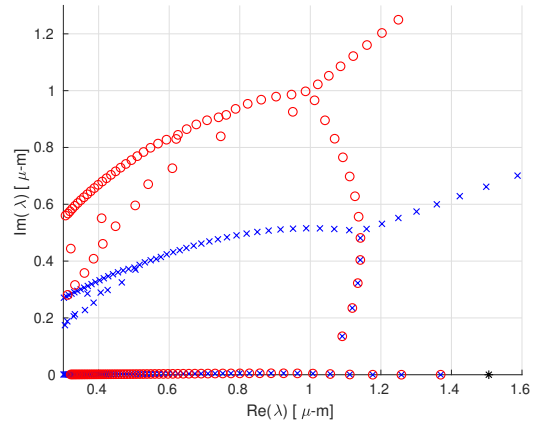
```
>> ylim([0,1.3])
```

The result is depicted in Fig. 11. Note that the target (or guess) resonance value is marked with a black star.

One can identify in Fig. 11, close to the real axis, a first family of resonances that remains unchanged in the two computations (circles and crosses are superimposed) and other branches of resonances that are shifted depending on the value of  $\sigma_0$ . Since the values of this latter family of resonances change with the PML parameters values, they are PML dependent and can therefore be related to the numerical approximation method. On the contrary, the first family of resonances that remains unchanged are the sought out resonances. We can also identify a short branch of resonances that remain unchanged but these resonances have a large imaginary part. They correspond to outer resonances [17]. Note that numerical investigations have shown that



(a) Resonance wavenumbers.



(b) Resonance wavelengths.

Figure 11: Shape of the spectrum of the Finite Difference matrices obtained for two computations with different values of the PML amplification coefficient  $\sigma_0$ : Blue crosses correspond to a computation with  $\sigma_0 = 0.445$  whereas red circles correspond to a computation with  $\sigma_0 = 1$ .

modifying the value of the PML regularity parameter  $\aleph$  do not imply a shift in the resonance values large enough to clearly distinguish between spurious and physical resonances.

## References

- [1] F. Olver, D. Lozier, R. Boisvert, C. Clark, NIST Handbook of Mathematical Functions, Cambridge University Press, 2010.
- [2] M. Abramowitz, I. A. Stegun, Handbook of Mathematical Functions: with Formulas, Graphs, and Mathematical Tables, Dover Publications, 1965.
- [3] A. Chiasera, Y. Dumeige, P. Féron, M. Ferrari, Y. Jestin, G. Nunzi-Conti, S. Pelli, S. Soria, G. Righini, Spherical whispering-gallery-mode microresonators, *Laser and Photonics Reviews* 4 (3) (2010) 457–482. [doi:10.1002/lpor.200910016](https://doi.org/10.1002/lpor.200910016).
- [4] M. Oxborrow, Traceable 2-D Finite-Element simulation of the whispering-gallery modes of axisymmetric electromagnetic resonators, *IEEE Transactions on Microwave Theory and Techniques* 55 (6) (2007) 1209–1218. [doi:10.1109/TMTT.2007.897850](https://doi.org/10.1109/TMTT.2007.897850).
- [5] A. Bermúdez, L. Hervella-Nieto, A. Prieto, A. Rodríguez, Perfectly Matched Layers for Time-Harmonic Second Order Elliptic Problems, *Arch. Computat. Methods Eng.* 17 (2010) 77–107. [doi:10.1007/s11831-010-9041-6](https://doi.org/10.1007/s11831-010-9041-6).
- [6] S. Kim, J. E. Pasciak, The computation of resonances in open systems using a perfectly matched layer, *Math. Comp.* 78 (267) (2009) 1375–1398. [doi:10.1090/S0025-5718-09-02227-3](https://doi.org/10.1090/S0025-5718-09-02227-3).
- [7] Z. Moitier, Etude mathématique et numérique des résonances dans un micro-résonateur optique, Ph.D. thesis, Université de Rennes, France (2019).
- [8] G. W. Stewart, A Krylov–Schur algorithm for large eigenproblems, *SIAM J. Matrix Anal. Appl.* 23 (3) (2001) 601–614. [doi:10.1137/S0895479800371529](https://doi.org/10.1137/S0895479800371529).
- [9] S. Balac, M. Dauge, Y. Dumeige, P. Féron, Z. Moitier, Mathematical analysis of whispering gallery modes in graded index optical micro-disk resonators, preprint hal-02157635 (2019).
- [10] C. C. Lam, P. T. Leung, K. Young, Explicit asymptotic formulas for the positions, widths, and strengths of resonances in Mie scattering, *Journal of the Optical Society of America B* 9 (9) (1992) 1585–1592.
- [11] V. S. Ilchenko, A. A. Savchenkov, A. B. Matsko, L. Maleki, Dispersion compensation in whispering-gallery modes, *Journal of the Optical Society of America A* 20 (1) (2003) 157–162.
- [12] S. Balac, M. Dauge, Z. Moitier, Asymptotics for 2D whispering gallery modes in optical micro-disks with radially varying index, arXiv preprint 2003.14315 (2020). [arXiv:2003.14315](https://arxiv.org/abs/2003.14315).
- [13] D. E. Winch, D. J. Ivers, J. P. R. Turner, R. J. Stening, Geomagnetism and Schmidt quasi-normalization, *Geophysical Journal International* 160 (2) (2005) 487–504. [doi:10.1111/j.1365-246X.2004.02472.x](https://doi.org/10.1111/j.1365-246X.2004.02472.x).
- [14] K. Dadashi, H. Kurt, K. Üstün, R. Esen, Graded index optical microresonators: analytical and numerical analyses, *J. Opt. Soc. Am. B* 31 (9) (2014) 2239–2245. [doi:10.1364/JOSAB.31.002239](https://doi.org/10.1364/JOSAB.31.002239).
- [15] B.-J. Li, P.-L. Liu, Numerical analysis of the whispering gallery modes by the finite-difference time-domain method, *IEEE Journal of Quantum Electronics* 32 (9) (1996) 1583–1587. [doi:10.1109/3.535362](https://doi.org/10.1109/3.535362).

- [16] I. S. Grudinin, N. Yu, Finite-element modeling of coupled optical microdisk resonators for displacement sensing, *J. Opt. Soc. Am. B* 29 (11) (2012) 3010–3014. doi:[10.1364/JOSAB.29.003010](https://doi.org/10.1364/JOSAB.29.003010).
- [17] J. Cho, I. Kim, S. Rim, G.-S. Yim, C.-M. Kim, Outer resonances and effective potential analogy in two-dimensional dielectric cavities, *Physics Letters A* 374 (17) (2010) 1893 – 1899. doi:[10.1016/j.physleta.2010.02.055](https://doi.org/10.1016/j.physleta.2010.02.055).
- [18] K. Chiang, Performance of the effective-index method for the analysis of dielectric waveguides, *Opt. Lett.* 16 (10) (1991) 714–716. doi:[10.1364/OL.16.000714](https://doi.org/10.1364/OL.16.000714).
- [19] M. Zworski, Resonances in physics and geometry, *Notices Amer. Math. Soc* 46 (3) (1999) 328.
- [20] J. Stratton, *Electromagnetic Theory*, An IEEE Press classic reissue, Wiley, 2007.
- [21] K. Atkinson, W. Han, *Spherical Harmonics and Approximations on the Unit Sphere: An Introduction*, *Lecture Notes in Mathematics*, Springer, 2012.
- [22] B. R. Johnson, Theory of morphology-dependent resonances: shape resonances and width formulas, *J. Opt. Soc. Am. A* 10 (2) (1993) 343–352. doi:[10.1364/JOSAA.10.000343](https://doi.org/10.1364/JOSAA.10.000343).

## Appendix

### A Physical and mathematical backgrounds

#### A.1 Maxwell's equations in a GRIN micro-resonator

A Whispering Gallery Mode (WGM) is characterized by a sinusoidal time varying electromagnetic field. The electric field  $\mathcal{E}$  and magnetic field  $\mathcal{H}$  can be represented in phasor notation as

$$\mathcal{E}(x, t) = \text{Re}(\mathbf{E}(x) e^{-i\omega t}) \quad (\text{A.1a})$$

$$\mathcal{H}(x, t) = \text{Re}(\mathbf{H}(x) e^{-i\omega t}) \quad (\text{A.1b})$$

where  $\omega$  denotes the optical wave frequency,  $t$  the time and  $x$  the position. The frequency  $\omega$  is not imposed by sources but it is one of the unknown of the resonance problem with  $\mathbf{E}$  and  $\mathbf{H}$ . In the sequel we denote by  $\Omega$  the bounded domain occupied by the dielectric cavity, by  $\Sigma$  its boundary and by  $\Omega_e$  the exterior domain:  $\Omega_e = \mathbb{R}^3 \setminus \overline{\Omega}$ . The electric field  $\mathbf{E}$  and magnetic field  $\mathbf{H}$  are complex valued solutions to the harmonic Maxwell's equations in  $\mathbb{R}^3$ :

$$\mathbf{curl} \mathbf{E} - i\omega\mu_0 \mathbf{H} = \mathbf{0} \quad (\text{A.2a})$$

$$\text{div} \mathbf{H} = 0 \quad (\text{A.2b})$$

$$\text{div}(\varepsilon_r \mathbf{E}) = 0 \quad (\text{A.2c})$$

$$\mathbf{curl} \mathbf{H} + i\omega\varepsilon_0 \varepsilon_r \mathbf{E} = \mathbf{0} \quad (\text{A.2d})$$

where  $\mu_0$  and  $\varepsilon_0$  denote respectively the magnetic permeability and the dielectric permittivity of vacuum and  $\varepsilon_r$  denotes the relative dielectric permittivity. We have  $\varepsilon_r = 1$  in  $\Omega_e$  and  $\varepsilon_r > 1$  in the cavity  $\Omega$ . In  $\Omega$ , the relative dielectric permittivity  $\varepsilon_r$  is generally position dependent. Equations (A.2) can be handled in  $\mathbb{R}^3$  when  $\mathbf{E}$  and  $\mathbf{H}$  refer to Schwartz's distributions or as regular functions in  $\Omega$  and  $\Omega_e$  with the following conditions at the interface  $\Sigma$ :

$$[\mathbf{H} \cdot \boldsymbol{\nu}] = 0 \quad [\varepsilon_r \mathbf{E} \cdot \boldsymbol{\nu}] = 0 \quad (\text{A.3a})$$

$$[\mathbf{H} \wedge \boldsymbol{\nu}] = \mathbf{0} \quad [\mathbf{E} \wedge \boldsymbol{\nu}] = \mathbf{0} \quad (\text{A.3b})$$

where  $\boldsymbol{\nu}$  denotes the unit outward normal to the boundary of  $\Omega$ , and the brackets refer to the jump across the interface of the quantity inside the brackets. We also need to specify some condition at infinity for  $\mathbf{H}$  and  $\mathbf{E}$ , typically an outgoing wave condition.

By taking the curl of equation (A.2a) and combining it with equation (A.2d), we obtain

$$\mathbf{curl} \mathbf{curl} \mathbf{E}(x) - k^2 N^2(x) \mathbf{E}(x) = \mathbf{0}$$

where  $k^2 = \omega^2 \mu_0 \varepsilon_0$  and  $N$  is the refractive index function defined by  $\varepsilon_r(x) = N^2(x)$ . From (A.2c) and the vector identity  $\text{div}(\varepsilon_r \mathbf{E}) = \varepsilon_r \text{div} \mathbf{E} + \mathbf{E} \cdot \nabla \varepsilon_r$  we deduce that

$$\text{div} \mathbf{E} = -\frac{\nabla N^2}{N^2} \cdot \mathbf{E}.$$

Then, using the vector identity  $\mathbf{curl} \mathbf{curl} \mathbf{E} = -\Delta \mathbf{E} + \nabla \text{div} \mathbf{E}$ , where  $\Delta$  refers to the vector Laplace operator, we finally obtain the following propagation equation in  $\Omega$  and  $\Omega_e$

$$\Delta \mathbf{E} + \nabla \left( \mathbf{E} \cdot \frac{\nabla N^2}{N^2} \right) + k^2 N^2 \mathbf{E} = 0. \quad (\text{A.4})$$

Similarly, by taking the curl of equation (A.2d) and by using the vector identity  $\mathbf{curl}(\varepsilon_r \mathbf{E}) = \varepsilon_r \mathbf{curl} \mathbf{E} + \nabla \varepsilon_r \wedge \mathbf{E}$  and equation (A.2a), we obtain that

$$-\mathbf{curl} \mathbf{curl} \mathbf{H} + \frac{\nabla N^2}{N^2} \wedge \mathbf{curl} \mathbf{H} + k^2 N^2 \mathbf{H} = 0.$$

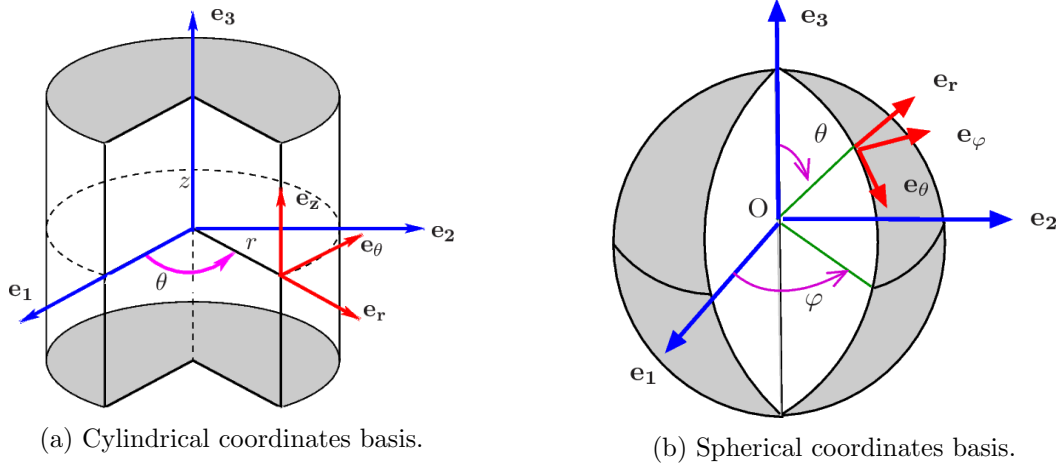


Figure 12: Notations for the cylindrical coordinates basis (left) and for the spherical coordinates basis (right).

Since  $\mathbf{H}$  is divergence free, the propagation equation for  $\mathbf{H}$  also reads

$$\Delta \mathbf{H} + \frac{\nabla N^2}{N^2} \wedge \mathbf{curl} \mathbf{H} + k^2 N^2 \mathbf{H} = 0. \quad (\text{A.5})$$

Our concern is the computation of WGM in a graded index micro-disk or micro-sphere where the refractive index  $N$  varies with the radial position  $r = |x|$  by solving equations (A.4) and (A.5) taking advantage of simplifications induced by the geometry of a sphere or a disk. An other assumption on the refractive index  $N$  is that it is represented by a smooth function of the radial position  $r$ . The mathematical approach for solving equations (A.4) and (A.5) is actually different for a micro-disk with radius  $R$  and for a micro-sphere with radius  $R$ , but the two formulations can be combined into a unique framework for the numerical approximation by the Finite Difference Method. We start by presenting the mathematical formulation for a micro-disk and then the formulation for the micro-sphere will be discussed.

## A.2 Mathematical model for WGM in a GRIN micro-disk

When the dielectric micro-cavity is a disk with a radial varying refractive index  $N$ , it is quite natural to exploit this feature by introducing the cylindrical coordinates basis  $(r, \theta, z)$ , see Fig. 12a. In the cylindrical vector basis  $(\mathbf{e}_r, \mathbf{e}_\theta, \mathbf{e}_z)$ , we have

$$\frac{\nabla N^2}{N^2} = \frac{2}{N} \partial_r N(r) \mathbf{e}_r = \partial_r (\ln(N^2)) \mathbf{e}_r.$$

Then, considering the expression of the vector Laplace operator in cylindrical coordinates, we obtain that component-wise equation (A.4) reads

$$\Delta E_r - \frac{2}{r^2} \partial_\theta E_\theta - \frac{1}{r^2} E_r + \partial_r E_r \partial_r (\ln(N^2)) + E_r \partial_r^2 \ln(N^2) + k^2 N^2 E_r = 0 \quad (\text{A.6a})$$

$$\Delta E_\theta + \frac{2}{r^2} \partial_\theta E_r - \frac{1}{r^2} E_\theta + \frac{1}{r} \partial_\theta E_r \partial_r (\ln(N^2)) + k^2 N^2 E_\theta = 0 \quad (\text{A.6b})$$

$$\Delta E_z + \partial_z E_r \partial_r (\ln(N^2)) + k^2 N^2 E_z = 0 \quad (\text{A.6c})$$

where  $\partial_r, \partial_\theta$  and  $\partial_z$  refer respectively to partial derivation with respect to the variables  $r, \theta$  and  $z$ , and  $\Delta$  refers to the scalar Laplace operator in polar coordinates. Similarly, we find that

equation (A.5) for  $\mathbf{H}$  reads

$$\Delta H_r - \frac{2}{r^2} \partial_\theta H_\theta - \frac{1}{r^2} H_r + k^2 N^2 H_r = 0 \quad (\text{A.7a})$$

$$\begin{aligned} \Delta H_\theta + \frac{2}{r^2} \partial_\theta H_r - \frac{1}{r^2} H_\theta - \frac{1}{r} \partial_r (\ln(N^2)) \partial_r (r H_\theta) \\ + \frac{1}{r} \partial_r (\ln(N^2)) \partial_\theta H_r + k^2 N^2 H_\theta = 0 \end{aligned} \quad (\text{A.7b})$$

$$\Delta H_z + \partial_r (\ln(N^2)) (\partial_z H_r - \partial_r H_z) + k^2 N^2 H_z = 0. \quad (\text{A.7c})$$

The main assumption in the model is that the electromagnetic field does not depend on the height variable  $z$  and the 3D geometrical problem setting can be reduced to a 2D one. This assumption and the resulting 2D problem can be seen as an approximation of the 3D one resulting from the use of the Effective Index Method [18]. Under this assumption, the magnetic field component  $H_z$  satisfies the following equation deduced from (A.7c)

$$\Delta H_z - \partial_r (\ln(N^2)) \partial_r H_z + k^2 N^2 H_z = 0$$

and this equation can be recast into

$$\operatorname{div} \left( \frac{1}{N^2} \nabla H_z \right) + k^2 H_z = 0.$$

Once  $H_z$  is known, the components  $E_r$  and  $E_\theta$  of the electric field can be deduced from Maxwell's equation (A.2d). Namely,

$$E_r(r, \theta) = \frac{i}{\omega \varepsilon r} \partial_\theta H_z(r, \theta) \quad (\text{A.8a})$$

$$E_\theta(r, \theta) = \frac{i}{\omega \varepsilon} \partial_r H_z(r, \theta). \quad (\text{A.8b})$$

We deduce from the boundary conditions (A.3b) combined with (A.8b) that  $H_z$  satisfies the following interface conditions across the cavity boundary  $\Sigma$ :

$$\left[ H_z \right] = 0, \quad \left[ \frac{1}{N^2} \frac{\partial H_z}{\partial \nu} \right] = 0.$$

Similarly, equation (A.6c) can be recast into

$$\Delta E_z(r, \theta) + k^2 N^2(r) E_z(r, \theta) = 0$$

and, under the assumption that the electromagnetic field does not depend on the height variable  $z$ , the components  $H_r$  and  $H_\theta$  of the magnetic field can be deduced from Maxwell's equation (A.2a) as

$$H_r(r, \theta) = \frac{1}{i\omega \mu_0 r} \partial_\theta E_z(r, \theta) \quad (\text{A.9a})$$

$$H_\theta(r, \theta) = -\frac{1}{i\omega \mu_0} \partial_r E_z(r, \theta). \quad (\text{A.9b})$$

Moreover, we deduce from the boundary conditions (A.3b) combined with (A.9b) that  $E_z$  satisfies the following interface conditions across the cavity boundary  $\Sigma$ :

$$\left[ E_z \right] = 0, \quad \left[ \frac{\partial E_z}{\partial \nu} \right] = 0.$$

Thus, as well known, we obtain that Maxwell's equations in polar coordinates split into two independent subsystems of equations. The first one involves the electromagnetic field components  $H_z$ ,  $E_r$  and  $E_\theta$  and it is referred as the TE modes subsystem. The second one involves

the electromagnetic field components  $E_z$ ,  $H_r$  and  $H_\theta$  and it is referred as the TM modes subsystem. Moreover, it is well known [19, 6] that the resonances wave-numbers are complex numbers with a negative imaginary part under the  $e^{-i\omega t}$  convention for harmonic time dependence of the electromagnetic field, see (A.1).

In the sequel, for the purposes of notation,  $\Omega$  (resp.  $\Omega_e$ ) will designate the trace of the three-dimensional micro-disk cavity  $\Omega$  (resp. of the exterior domain  $\Omega_e$ ) in the plane  $z = 0$ . We denote by  $L^2_{\text{loc}}(\mathbb{R}^2)$  the Lebesgue set of locally square integrable functions in  $\mathbb{R}^2$  and by  $H^2(\Omega)$  (resp. by  $H^2_{\text{loc}}(\Omega_e)$ ) the Sobolev space of square integrable functions in  $\Omega$  (resp. locally square integrable functions in  $\Omega_e$ ) with all derivatives up to order 2 in  $L^2(\Omega)$  (resp. in  $L^2_{\text{loc}}(\Omega_e)$ ). We introduce the space of functions

$$D(\mathbb{R}^2) = \{u \in L^2_{\text{loc}}(\mathbb{R}^2) \mid u|_{\Omega} \in H^2(\Omega), u|_{\Omega_e} \in H^2_{\text{loc}}(\Omega_e)\}. \quad (\text{A.10})$$

For a varying refractive index  $N$ , the resonance problems for TE and TM modes in the cavity  $\Omega$  can be gathered into a unique form by introducing a mode selection index  $p$  such that  $p = -1$  for TE modes and  $p = +1$  for TM modes. This resonance problem reads: find  $(k, u) \in \mathbb{C} \times D(\mathbb{R}^2)$  such that  $u \neq 0$ ,  $\text{Im}(k) < 0$  and

$$-\text{div}(N^{p-1} \nabla u) - k^2 N^{p+1} u = 0 \quad \text{in } \Omega \text{ and } \Omega_e \quad (\text{A.11a})$$

$$\left[ u \right] = 0 \quad \text{across } \Sigma \quad (\text{A.11b})$$

$$\left[ N^{p-1} \frac{\partial u}{\partial \nu} \right] = 0 \quad \text{across } \Sigma \quad (\text{A.11c})$$

with an appropriate outgoing wave condition at infinity. For TE modes, in the cylindrical basis, the unknown  $u$  is the component  $H_z$  of the magnetic field whereas for TM modes the unknown  $u$  is the component  $E_z$  of the magnetic field and the resonance wavelength  $\lambda$  is connected to the resonance wave-number  $k$  through the relation  $\lambda = 2\pi/k$ .

When considering a disk shaped cavity with a radially varying refractive index  $N$ , the Fourier approach can be used to solve the resonance problem (A.11). The eigenfunction  $u$  for a solution  $(k, u)$  to problem (A.11) is expanded in polar coordinates as

$$u(r, \theta) = \sum_{m \in \mathbb{Z}} u_m(r) e^{im\theta}. \quad (\text{A.12})$$

We can deduce from (A.11) the problem satisfied by  $u_m$ . To this end, let  $L^2_{\text{loc}}(\mathbb{R}^+, r dr)$  denotes the Lebesgue set of locally square integrable functions in  $\mathbb{R}^+$  with respect to the measure  $r dr$  and let  $H^2(\mathbb{R}^+, r dr)$  (resp.  $H^2_{\text{loc}}(]R, +\infty[, r dr)$ ) denotes the Sobolev space of square integrable functions in  $]0, R[$  (resp. locally square integrable functions in  $]R, +\infty[$ ) with all derivatives up to order 2 in  $L^2(]0, R[, r dr)$  (resp. in  $L^2_{\text{loc}}(]R, +\infty[, r dr)$ ). We introduce the space of functions

$$D(\mathbb{R}^+, r dr) = \{v \in L^2_{\text{loc}}(\mathbb{R}^+, r dr) \mid v|_{]0, R[} \in H^2(]0, R[, r dr), v|_{]R, +\infty[} \in H^2_{\text{loc}}(]R, +\infty[, r dr)\}.$$

From (A.12), it is found that solutions to problem (A.11) are obtained from the solutions to the following family of 1D problems: Find  $(k, u_m) \in \mathbb{C} \times D(\mathbb{R}^+, r dr)$  such that  $\text{Im}(k) < 0$ ,  $u_m \neq 0$  and

$$-u''_m(r) - \frac{1}{r} \left( 1 + (p-1)r \frac{N'(r)}{N(r)} \right) u'_m(r) + \left( \frac{m^2}{r^2} - k_m^2 N^2(r) \right) u_m(r) = 0 \quad \text{in } ]0, R[ \text{ and } ]R, +\infty[ \quad (\text{A.13a})$$

$$\left[ u_m(r) \right]_{r=R} = 0 \quad (\text{A.13b})$$

$$\left[ N^{p-1}(R) u'_m(R) \right]_{r=R} = 0 \quad (\text{A.13c})$$

where here the prime symbol refers to the derivative of a function of a real variable. Note that for  $m \neq 0$ , the singularity  $\frac{m}{r^2}$  in (A.13a) implies that the solution must satisfy the Dirichlet condition  $u_m(0) = 0$ . For  $m = 0$ ,  $u_m$  must satisfy instead the Neumann boundary condition  $u'_m(0) = 0$ . In the sequel, we will only consider the case when  $m \neq 0$  since the case  $m = 0$  is of poor practical interest.

In the exterior domain  $]R, +\infty[$ , equation (A.13a) reads

$$u_m''(r) - \frac{1}{r}u_m'(r) + \left(\frac{m^2}{r^2} - k_m^2\right) u_m(r) = 0 \quad (\text{A.14})$$

Introducing the variable  $x = kr$  and the new unknown  $v_m(x) = u_m(r)$ , equation (A.14) in the new variable  $x$  for  $v_m$  reads

$$x^2 v_m''(x) + x v_m'(x) + (x^2 - m^2) v_m(x) = 0. \quad (\text{A.15})$$

This second order ordinary differential equation is referred to as Bessel's equation of order  $m$ . The space of solutions admits a basis formed e.g. of the two linearly independent Hankel functions  $H_m^{(1)}$  and  $H_m^{(2)}$ . As well known, under the  $e^{-i\omega t}$  convention for harmonic time dependence of the electromagnetic field, see (A.1), Hankel function  $H_m^{(1)}$  represents outgoing waves whereas  $H_m^{(2)}$  represents ingoing waves. Since WGM correspond to outgoing waves, the condition at infinity for problem (A.13) reads

$$u_m(r) \propto H_m^{(1)}(k_m r) \text{ as } r \rightarrow +\infty \quad (\text{A.16})$$

where the notation  $\propto$  means ‘‘proportional to’’.

### Mode indexes for a micro-disk

A solution  $(k_m, u_m)$  to problem (A.13)–(A.16) is referred to as a mode of the micro-disk cavity with *polar mode index*  $m$ . For a given mode index  $m$ , problem (A.13) has a sequence of solutions, indexed by a second index  $j$ , termed the *radial mode index*. Moreover, one can see from problem (A.13) that in a GRIN micro-disk resonator the resonances have multiplicity 2 since the two indexes  $\pm m$  provide the same resonance wave-number  $k$ , the modes being expressed as a linear combination of  $u_m(r) e^{im\theta}$  and its complex conjugate  $\overline{u_m(r)} e^{-im\theta}$ . Thus, we will restrict the discussion to positive integer values of  $m$ .

We have depicted in Fig. 13 the electric field amplitude of the TE mode with mode indexes  $m = 20$  and  $j = 3$  in a micro-disk with constant refractive index. Note that the evanescent part of the field is not represented. (A similar pattern is obtained for the magnetic field amplitude and for the TM mode.) We can observe that  $2m$  is the number of lobes (local extrema) whereas  $j$  is the number of lobes in the radial direction.

### A.3 Mathematical model for WGM in a GRIN micro-sphere

It is well known that for a dielectric sphere with constant dielectric permittivity, Maxwell's harmonic equations (A.2) can be solved analytically using Hansen's method [20]. When the refractive index  $N$  of the dielectric sphere varies in the radial direction, it is still possible to construct solutions to the vector Helmholtz equation (A.4) and (A.5). Drawing on Hansen approach for the dielectric sphere with constant refractive index, we define for  $\ell \in \mathbb{N}$  and  $m \in \mathbb{Z}$  such that  $-\ell \leq m \leq \ell$ , the following Vector Harmonics

$$\mathbf{M}_\ell^m(r, \theta, \varphi) = \mathbf{curl} \left( v(r) Y_\ell^m(\theta, \varphi) \mathbf{e}_r \right) \quad (\text{A.17a})$$

$$\mathbf{N}_\ell^m(r, \theta, \varphi) = \frac{1}{kN(r)} \mathbf{curl} \mathbf{M}_\ell^m(r, \theta, \varphi) \quad (\text{A.17b})$$

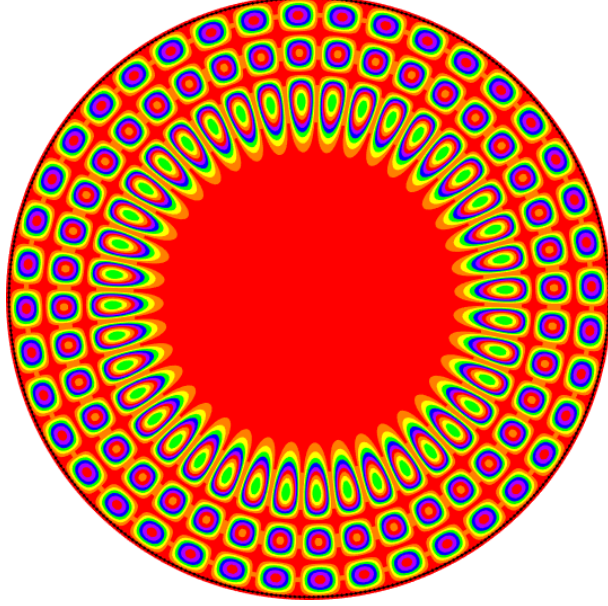


Figure 13: Electric field amplitude of the TE mode with mode indexes  $m = 20$  and  $j = 3$  in a micro-disk with constant refractive index.

where  $v$  denotes at this stage an unknown function and  $Y_\ell^m$  the Spherical Surface harmonics of degree  $\ell$  and order  $m$  [21] defined in terms of Associated Legendre function  $P_\ell^m$  as

$$Y_\ell^m(\theta, \varphi) = C_{\ell m} P_\ell^m(\cos(\theta)) e^{im\varphi} \quad \text{where } C_{\ell m} = \sqrt{\frac{(2\ell + 1)(\ell - m)!}{4\pi(\ell + m)!}} \quad (\text{A.18})$$

for all integers  $\ell$  and  $m$  such that  $-\ell \leq m \leq \ell$ .

In the spherical coordinates basis, we have

$$\mathbf{M}_\ell^m = \frac{1}{r} \begin{pmatrix} 0 \\ \frac{1}{\sin(\theta)} v \partial_\varphi Y_\ell^m \\ -v \partial_\theta Y_\ell^m \end{pmatrix}$$

and, since  $\Delta Y_\ell^m + \frac{\ell(\ell+1)}{r^2} Y_\ell^m = 0$ , we find that

$$\mathbf{curl} \mathbf{curl} \mathbf{M}_\ell^m = \begin{pmatrix} 0 \\ -\frac{1}{r \sin(\theta)} \left( \partial_r^2(rv) - \ell(\ell+1) \frac{1}{r} v \right) \partial_\varphi Y_\ell^m \\ \frac{1}{r} \left( \partial_r^2(rv) - \ell(\ell+1) \frac{1}{r} v \right) \partial_\theta Y_\ell^m \end{pmatrix}.$$

It follows that if  $v$  solves the scalar equation

$$-\frac{1}{r} \partial_r^2(rv(r)) + \left( \frac{\ell(\ell+1)}{r^2} - k^2 N^2(r) \right) v(r) = 0 \quad (\text{A.19})$$

then  $\mathbf{curl} \mathbf{curl} \mathbf{M}_\ell^m - k^2 N^2 \mathbf{M}_\ell^m = \mathbf{0}$ . Moreover,

$$\text{div}(\varepsilon_r \mathbf{M}_\ell^m) = \mathbf{M}_\ell^m \cdot \nabla \varepsilon_r + \varepsilon_r \text{div} \mathbf{M}_\ell^m = \partial_r \varepsilon_r \mathbf{M}_\ell^m \cdot \mathbf{e}_r = 0.$$

Therefore  $\mathbf{M}_\ell^m$  solves problem (A.2) for the electric field  $\mathbf{E}$  in the two domains  $\Omega$  and  $\Omega_e$ . From (A.2a), the magnetic field is then expressed as  $\mathbf{H} = -\frac{i}{\omega \mu_0} k N \mathbf{M}_\ell^m$ . Such a solution corresponds

to the so-called TE modes for the dielectric sphere [3]. Equation (A.19) is to be considered in  $\Omega$  and  $\Omega_e$  (where  $N = 1$ ) together with the following conditions across the sphere boundary for  $v$  deduced from (A.3):

$$\left[ v(r) \right]_{r=R} = 0, \quad \left[ v'(r) \right]_{r=R} = 0. \quad (\text{A.20})$$

A similar development can be done by considering the Vector Harmonics

$$\mathbf{P}_\ell^m = \frac{1}{kN} \mathbf{N}_\ell^m = \begin{pmatrix} \frac{\ell(\ell+1)}{k^2 N^2} \frac{v}{r} Y_\ell^m \\ \frac{1}{k^2 N^2} \frac{1}{r} \partial_\theta Y_\ell^m \partial_r (rv) \\ \frac{1}{k^2 N^2} \frac{1}{r \sin(\theta)} \partial_\varphi Y_\ell^m \partial_r (rv) \end{pmatrix}. \quad (\text{A.21})$$

We obtain that if  $v$  solves the scalar equation

$$-\frac{1}{r} \partial_r^2 (rv(r)) + \frac{2}{r} \frac{N'(r)}{N(r)} \partial_r (rv(r)) + \left( \frac{\ell(\ell+1)}{r^2} - k^2 N^2(r) \right) v(r) = 0 \quad (\text{A.22})$$

then  $\mathbf{curl} \mathbf{curl} \mathbf{P}_\ell^m - k^2 N^2 \mathbf{P}_\ell^m = \mathbf{0}$ . Moreover,

$$\text{div} (\varepsilon_r \mathbf{P}_\ell^m) = \frac{1}{k^2} \text{div} (\mathbf{curl} \mathbf{M}_\ell^m) = 0.$$

Therefore,  $\mathbf{P}_\ell^m$  also solves problem (A.2) for the electric field  $\mathbf{E}$  and from (A.2a), the magnetic field is found to be  $\mathbf{H} = -\frac{i}{\omega \mu_0} \mathbf{M}_\ell^m$ . Such a solution corresponds to the so-called TM modes for the dielectric sphere [3]. Equation (A.22) is to be considered in  $\Omega$  and  $\Omega_e$  (where  $N = 1$ ) together with the following conditions across the sphere boundary for  $v$  deduced from (A.3):

$$\left[ v(r) \right]_{r=R} = 0, \quad \left[ \frac{1}{N^2} \partial_r (rv) \right]_{r=R} = 0. \quad (\text{A.23})$$

Both for TE and TM modes, at infinity,  $v$  must satisfy the following outgoing radiation condition:  $v(r) \propto h_\ell^{(1)}(kr)$  as  $r \rightarrow +\infty$  where  $h_\ell^{(1)}$  denotes the Spherical Hankel's function of the first kind [1, 2].

For a varying refractive index  $N$ , the resonance problems for TE and TM modes in the cavity  $\Omega$  can be gathered into a unique form by introducing a mode selection index  $p$  such that  $p = 1$  for TE modes and  $p = -1$  for TM modes. Introducing as new unknown the so-called Debye potential  $S_\ell$  [22] such that  $S_\ell(r) = kr v(r)$ , the resonance problem reads: find  $(k, S_\ell) \in \mathbb{C} \times \mathcal{D}(\mathbb{R}^+, r dr)$  such that  $\text{Im}(k) < 0$ ,  $S_\ell \neq 0$  and

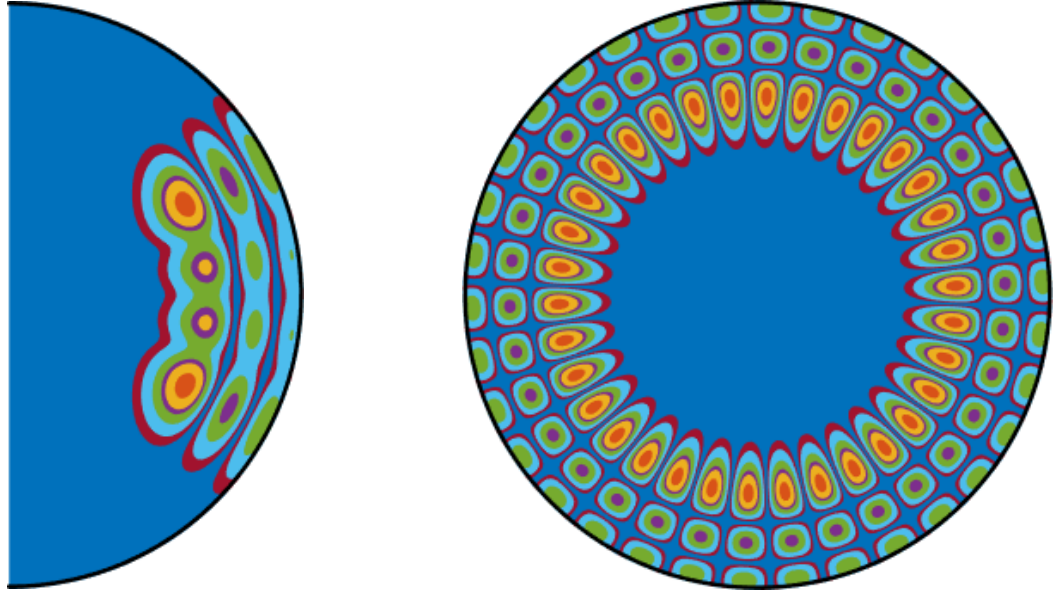
$$S_\ell''(r) + (p-1) \frac{N'(r)}{N(r)} S_\ell'(r) + \left( k^2 N^2(r) - \frac{\ell(\ell+1)}{r^2} \right) S_\ell(r) = 0 \quad \text{in } ]0, R[ \text{ and } ]R, +\infty[ \quad (\text{A.24a})$$

$$\left[ S_\ell(r) \right]_{r=R} = 0 \quad (\text{A.24b})$$

$$\left[ N^{p-1}(r) S_\ell'(r) \right]_{r=R} = 0 \quad (\text{A.24c})$$

At infinity,  $S_\ell$  must satisfy the following outgoing radiation condition:  $S_\ell(r) \propto kr h_\ell^{(1)}(kr) = \xi_\ell(kr)$  as  $r \rightarrow +\infty$ , where  $h_\ell^{(1)}$  denotes the Spherical Hankel's function of the first kind and  $\xi_\ell$  denotes the Ricatti-Bessel function.

Note that for  $\ell \neq 0$ , the singularity  $\frac{\ell(\ell+1)}{r^2}$  in (A.24a) implies that the solution must satisfy the Dirichlet condition  $S_\ell(0) = 0$  and for  $\ell = 0$ ,  $S_\ell$  must satisfy instead the Neumann boundary condition  $S_\ell'(0) = 0$ .



(a) View in the azimuth plane  $\varphi = 0$ .

(b) View in the polar plane  $\theta = \frac{\pi}{2}$ .

Figure 14: Electric field amplitude of the TE mode with mode indexes  $\ell = 20$ ,  $m = 17$  and  $n = 3$  in a micro-sphere with constant refractive index.

#### Mode indexes for a micro-sphere

A mode  $(k, S_\ell)$  is described in terms of three integers. The first two are the integer  $\ell$  involved in (A.24a) and the integer  $m$  involved in the expression of the electromagnetic field of the mode, see (A.17). Note that this underscores a mode degeneracy since there exist  $2\ell + 1$  modes with the same values of  $\ell$  and therefore with the same resonance  $k$ , but with a different value for  $m$  and therefore with a different expression for the electromagnetic field. The *polar mode number*  $\ell$  (we use the terminology introduced in [3]) corresponds to the number of wavelengths taken to travel around the sphere. The index  $m$  is called the *azimuthal mode number*. It can take  $2\ell + 1$  values from  $-\ell$  to  $\ell$  and it is related to the sinusoidal variation of the mode with the azimuthal angle  $\varphi$ , see Fig 12b. The third integer, denoted by  $n$ , labels the solutions to problem (A.24) for a fixed value of  $\ell$ . It is referred to as the *radial mode number* and corresponds to the number of intensity maxima of the mode in the radial direction  $\mathbf{e}_r$ .

We have depicted in Fig. 14 the electric field amplitude of the TE mode with mode indexes  $\ell = 20$ ,  $m = 17$  and  $n = 3$  in a micro-sphere with constant refractive index. Note that the evanescent part of the field is not represented. (A similar pattern is obtained for the magnetic field amplitude and for the TM mode.) More precisely, Fig. 14a shows the electric field amplitude in the azimuth plane  $\varphi = 0$  and Fig. 14b shows the electric field amplitude in the polar plane  $\theta = \frac{\pi}{2}$ . We can observe in Fig. 14b that  $2\ell$  is the number of lobes (local extrema) in the equatorial plane  $\theta = \frac{\pi}{2}$  whereas  $n$  is the number of lobes in the radial direction. One can also observe in Fig. 14a that  $\ell + 1 - |m| = 4$  is the number of lobes in a meridian plane. (We can also observe in Fig. 14a that  $n$  is the number of lobes in the radial direction.)